Ph.D Thesis

# Matching and Visualization for Refitting Materials of Stone Tool Based on 3D Measured Point Cloud

Xi Yang

Department of Design and Media Technology
Graduate School of Engineering
Iwate University

March 2018

# Abstract

In Japan, lithic materials are most important evidences of archaeological research in the Palaeolithic and Jomon periods. Most organics, such as bones or wood, are easy to decay, due to the hot and humid weather and acidic ground soil. To make a stone tool, the edge of a rock is struck repeatedly with a pebble, and flake pieces in various sizes are obtained. These pieces are called lithic refitting materials. The flakes are pieces peeled for adjusting the core shape, while the core is the rock left as a raw material for a stone tool when flakes are peeled. Refitting lithic materials is the most important research work for analyzing human activities of that period. By this work, the manufacturing process of stone tools can be restored and human activities in the ancient times can be conjectured. The original form of relics can be known, while, additionally these reassembled stone tools can also have educational values as exhibition materials at history museums. However, reassembly of stone tools is a complex and hard task, it consumes a lot of manpower and time. In order to efficiently process massive stone tools, this thesis studied computer graphics techniques to assist this archaeological research. This work is mainly composed of the following two aspects: lithic materials matching and assembly instruction visualization.

In recent decades, a large number of methods have been presented to solve various registration or matching problems, however, few methods have been successfully applied to the matching of flakes. In the previous work, it is possible to process refitting materials from a single stone core, while it is impossible to finish them from multiple stone cores. By improving this method, this thesis proposed a new method for refitting mixture lithic materials from multiple stone cores by matching flake surfaces. First, each of the input point clouds of lithic materials is segmented and simplified to obtain flake surfaces.

Then, according to several refitting principles in archaeology, the lithic materials are matched starting from a stone core by searching the best matching flake surface. Additionally, the flake surfaces of matched lithic materials are detected and reconstructed. The matching process is repeated until all data are matched.

In the next research, independently from the polygon mesh, a new algorithm is proposed to process pairwise matching of stone tools based on contour points and mean normals of regions on all flake surfaces, according to the characteristics of the flake models. The input of our method is a pair of flake models from the point cloud. First, the normal vectors are calculated for each point. Second, each flake surface is segmented and uniformly downsampled. After that, the contour points are extracted. Finally, the flake surface pair with the best matching is rapidly identified based on the contour points, and further matching is conducted using the nearest point sets.

For studying stone tools, repeating assembly and separation of stone tools is an inevitable process. However, ambiguous traditional 2D illustrations are commonly used to instruct this process. The 3D exploded view is an effective way for instructing the assembly, and it has been widely used in many fields, while seldom being used in archaeology. We applied a powerful presentation technique, 3D exploded view, to stone tool models. Based on the refitting results of lithic materials, a method is studied to calculate relationships and directions of stone tool models for generating exploded graphs with point clouds. In addition, the assembly and separation sequences are computed. According to archaeological conventions, the animation of the rotating separation of a flake is also generated. Moreover, lithic knapping methods and relic excavation reports are analyzed to evaluate the difference of flake knapping sequences between the contents of the report and automatic generation.

We have implemented the proposed methods and tested with lithic material 3D models. Two groups are efficiently finished through our matching method by refitting materials from the mixture of several groups. The limitation of this method has been solved by the next research. These experimental examples indicated that the matching methods can achieve superior matching results. After that, the explosion graphs of two groups are generated, and the assembly and separation sequences are computed and analyzed. The experimental results of stone tool assemblies indicate that 3D visualization

technology can assist in the efficient research of assembly and separation instruction of stone tools for chipped stone tools.

English translation of archaeological words in this thesis according to [91].

# Acknowledgements

I would like to express my gratitude to all those who helped me during this research.

First of all, I would like to extend my sincere gratitude to my supervisor, Prof. Kouichi Konno. for his patient academic guidance and a great support in the life. I gratefully acknowledge the help of Assoc. Prof. Katsutsugu Matsuyama. His advice is always accurate and concise. I am also deeply indebted to Mr. Shin Yokoyama and Dr. Fumito Chiba for their research cooperation.

I am deeply grateful to Prof. Takamitsu Tanaka and Prof. Tadahiro Fujimoto who discussed in revising this thesis. Additionally, I would like to thank Mrs. Hikaru Kaketa and Mr. Morimichi Furudate who helped improve research environment. I deeply appreciate the help from my teachers and friends, Prof. Zhiyi Zhang, Assoc. Prof. Shaojun Hu and Dr. Zepeng Wang.

Last but not the least, my gratitude also extends to my parents, my wife Jingbo He and my baby Yezhen Yang who have been assisting, supporting and caring for me all of my life.

Feelings of fulfillment are fleeting, so I am always in entangled, fear and suffering, but probably that will keep me going.

# Contents

**List of Figures** vii

**List of Tables** ix

**1 Introduction** 1
- 1.1 Stone Tool Assembles . . . 1
- 1.2 Thesis Outline . . . 4

**2 Related Works** 6
- 2.1 Technologies and Applications . . . 6
- 2.2 Previous Works . . . 8
  - 2.2.1 Data Acquisition . . . 8
  - 2.2.2 Simplification . . . 9
  - 2.2.3 Matching . . . 10

**3 Matching** 12
- 3.1 Overview . . . 12
- 3.2 Related Works . . . 12
  - 3.2.1 Matching and Registration . . . 12
  - 3.2.2 Flake Surfaces . . . 15
- 3.3 Matching Based on Mesh . . . 16
  - 3.3.1 Algorithm Overview . . . 16
  - 3.3.2 Segmentation and Simplification of Flake Surfaces . . . 16
  - 3.3.3 Mixture Matching . . . 17
  - 3.3.4 Flake Surface Reconstruction . . . 20
  - 3.3.5 Experimental Results . . . 25

3.3.6 Limitation . . . . . 28
3.4 Matching Based on Point Cloud . . . . . 35
3.4.1 Overview . . . . . 35
3.4.2 Preparation Work . . . . . 35
3.4.3 Pairwise Matching . . . . . 36
3.4.4 Results . . . . . 39
3.5 Discussion . . . . . 40

**4 Visualization** **46**
4.1 Overview . . . . . 46
4.2 Related Works . . . . . 47
4.2.1 Lithic Technology and Traditional Illustration . . . . . 47
4.2.2 3D Illustrative Visualization . . . . . 48
4.3 Visualization Instruction . . . . . 50
4.3.1 Our System . . . . . 50
4.3.2 Constructing Explosion Graph . . . . . 50
4.3.3 Generating Assembly Sequence and Interactive Control 52
4.3.4 Flake Knapping Sequence Analysis . . . . . 52
4.3.5 Exporting Animation . . . . . 54
4.4 Results and Evaluation . . . . . 54
4.4.1 Results . . . . . 54
4.4.2 Evaluation . . . . . 57
4.5 Summary . . . . . 59

**5 System Architecture** **67**
5.1 The Preparation Work Tool . . . . . 67
5.2 Matching System . . . . . 69

**6 Conclusions and Future Work** **72**
6.1 Conclusions . . . . . 72
6.2 Future Work . . . . . 73

**Bibliography** **85**

**List of Publications** **i**

# List of Figures


1.1 Chipped stone tool manufacture. . . . . 2
1.2 A photo of an excavation site showing scattered stone tools. . 3
1.3 Excavated flake pieces. . . . . 4

2.1 Point Cloud Techniques. . . . . 7
2.2 Scanning Device. . . . . 9
2.3 Simplified results of the new method. . . . . 10
2.4 Previous works about matching. . . . . 11

3.1 Matching by flake surfaces. . . . . 15
3.2 A case of making a stone tool. . . . . 18
3.3 D2 distribution on four flake surfaces. . . . . 21
3.4 Computing method of normalized distance. . . . . 22
3.5 Matching algorithm. . . . . 23
3.6 Searching reconstruction flake surfaces. . . . . 24
3.7 43 experiment data. . . . . 25
3.8 Results of segmentation. . . . . 26
3.9 Results of Simplification. . . . . 27
3.10 Result of pairwise matching. . . . . 30
3.11 Result of reconstruction. . . . . 31
3.12 An actual picture and the result of final matching for group 1. 32
3.13 An actual picture and the result of final matching for group 2. 33
3.14 Limitation of our method. . . . . 34
3.15 Segmenting flake surfaces from a single flake. . . . . 36
3.16 Construction of 4 points for source $S$ and target $T$ surfaces. . 37
3.17 Matching two contour sections. . . . . 38
3.18 Comparison results. . . . . 41
3.19 The first flake pair. . . . . 42

3.20 The second flake pair. . . . . 43
3.21 The third flake pair. . . . . 44
3.22 An example of a matching assembly of seven stone tools. . . . 45

4.1 Making a stone tool. . . . . 48
4.2 Traditional illustration of stone tools in a relic excavation report. 49
4.3 Original input models and the generated adjacent relationships. 51
4.4 The directed relationship graph and generated hierarchical tree. 52
4.5 Calculation the coordinate system of a flake surface from adjacent points. . . . . 53
4.6 A cross section of the assembly of stone tools. . . . . 54
4.7 Interactively generating the assembly order of stone tools. . . 55
4.8 A cross section. . . . . 56
4.9 A relationship graph including the reconstruction relationships. 57
4.10 An example from the relic excavation report. . . . . 57
4.11 Rotating separation of a flake . . . . . 58
4.12 Calculating the transform matrix of separation. . . . . 59
4.13 Original models of group 1 and group 2. . . . . 60
4.14 3D exploded diagram of group 1. . . . . 61
4.15 3D exploded diagram of group 2. . . . . 62
4.16 3D relationship graph. . . . . 63
4.17 Assembly instruction with a step-by-step guide for group 2. . . 64
4.18 Flake knapping sequence instruction with a step-by-step guide for group 2. . . . . 65
4.19 The reassembly times. . . . . 66
4.20 The result of questionnaire. . . . . 66

5.1 The preparation work tool. . . . . 69
5.2 The folder structure. . . . . 70
5.3 The workflow of system. . . . . 70
5.4 Waiting viewer. . . . . 71
5.5 Matching viewer. . . . . 71

# List of Tables

3.1 Results of Simplification. . . . . 28
3.2 Matching of group 1. . . . . 28
3.3 Matching of group 2. . . . . 29
3.4 Flake matching performance of the proposed method. . . . . 40

# Chapter 1

# Introduction

## 1.1 Stone Tool Assembles

Stone tools indicate a variety of cutting tools or weapons made by ancients. In archaeology, there is no uniform standard across the world for the classification, typology, analysis and other research of stone tools [36]. For the Palaeolithic and Jomon periods of Japan, they are mainly divided into chipped stone tools and polished stone tool according to manufacturing techniques. To make a chipped stone tool, the edge of a rock is struck repeatedly with a pebble, and flake pieces of various sizes are obtained, as shown in Figure 1.1. These pieces are called lithic materials, the flakes are the pieces peeled for adjusting the core shape, the core is the rock left as a raw material for a stone tool when flakes are peeled [55].

In archaeology, archaeological materials are very important evidences of human activity research [90]. With the data, archaeologists can study the time's technical characteristics, sociocultural backgrounds, habits and other significant subjects. However, in Japan, the most of excavated relics are just stone tools because the weather is almost hot and humid and the ground soil is acidic. In this environment, the most organics, such as bones or woods, except stones have perished easily. Hence, lithic materials are main objects for tracing human activities in the ancient times [55].

Reassembling stone tools from a raw rock is a necessary process for finishing and analyzing excavated relics, as these relics are scattered and distributed

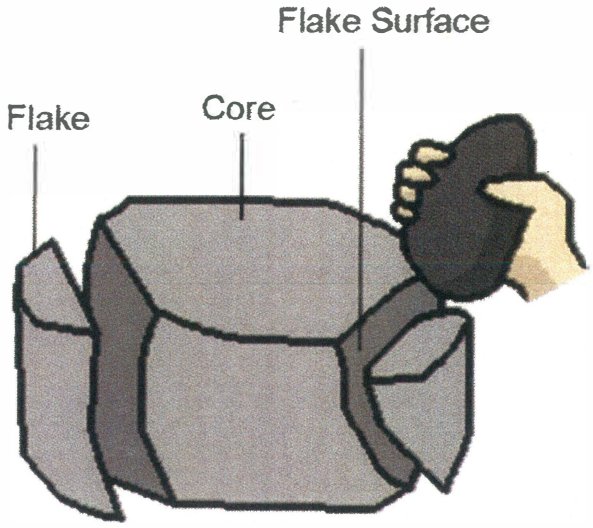


Figure 1.1: Chipped stone tool manufacture.

in sites similar to those shown in Figure 1.2 [63]. The refitting of flakes allows their manufacturing process to be determined, and the technical characteristics to be analyzed. Then, the original form of relics that have been used can be known, and hence, conjectures can be made regarding human activities during that time. Reassembled lithic materials have educational values as exhibition materials at history museums. Furthermore, the relationships between neighboring sites can be determined by the distribution of assembled stone tools. Based on this, it is possible to clarify a part of the behavioral patterns of people in ruins [90].

Refitting lithic materials is a complex and hard task and it may consume a lot of time and manpower. Dealing with these problems by computer algorithms is a solution. Many methods have been proposed for feature extraction and analysis of lithic [70, 74], while our work focuses on the refitting of stone tools using digital technology that few researches have proposed. Therefore, we want to study computer graphics techniques to assist in finishing research of lithic refitting materials rapidly and accurately. However, it is extraordinarily difficult to finish and analyze excavated relics [90] as shown in Figure 1.3. In Japan, even the conjoining status of lithic materials has been analyzed since 1960 [41], no superb solution algorithms have been proposed yet for refitting lithic materials, especially for the mixture lithic materials with several different stone cores.

Figure 1.2: A photo of an excavation site showing scattered stone tools.

After searching matching flakes, repeating assembly and separation stone tools is an inevitable process in the study. However, traditional archaeological illustrations have largely affected the efficiency of assembly operations. This is because it is extremely difficult to identify 3D objects by using 2D scale drawings or pictures. In addition, the process of 2D scale drawings is time-consuming. On the other hand, 3D exploded view diagrams have been widely used in many industries since the introduction of assembly instruction visualization in 2003 [8], including furniture products, CAD models, and medical volume data. In the field of cultural heritage, there are many assembly models of relic restoration. The technologies and tools of computer graphics can effectively assist archaeologists in the analysis of archaeological findings via reconstruction and visualization [61, 82]; however, in spite of the numerous reassembling methods and pairwise matching algorithms proposed for fractured objects [40, 68, 72], no application of assembly instruction has been developed for archaeological research.

To solve the above problems, in this thesis, new methods are proposed for refitting mixture lithic materials by matching flake surfaces, and interactively visualizing assembly instruction for 3D stone tool models in order to improve the user experience. The experiments show our proposed method could obtain superb results for the models of lithic material.

Figure 1.3: Excavated flake pieces.

## 1.2 Thesis Outline

This thesis is composed of 6 chapter including this chapter, the outline of each chapter is organized as follows.

In Chapter 2, the related algorithms in computer graphics are summarized, then applications in archaeology and cultural heritage are introduced. We also explained the previous works for refitting lithic materials.

Chapter 3 described our matching work in detail. The related works in matching and registration are introduced. With analyzing the characteristics of flake surfaces, a new method for mixture refitting lithic materials is proposed. And then, a point cloud based algorithm is developed to solve the limitation of the previous method and make matching processing more efficient.

Chapter 4 developed a visualization method to instruct the reassembly and separation work of lithic materials. The traditional illustrations and 3D diagrams are compared, the visualization instruction method is studied according to archaeology rules. Comparison experiments are employed to evaluate our proposed method.

Chapter 5 explained the programming details to implement the proposed algorithms.

Chapter 6 summarized our work of matching and visualization, and the future work is proposed.

# Chapter 2

# Related Works

## 2.1 Technologies and Applications

Related works of lithic material research mainly included two fields: computer graphics in archaeology [61] and computer graphics in cultural heritage [72]. For using computer graphics technicals to assist in processing cultural relic, the actual objects need to be measured to obtain 3D model data by laser scanner [49] or camera devices. Point cloud is the basic representation for 3D model. It shows geometric information of models. Polygon mesh is one of the ways to reconstruct surface of model [37], it can be constructed by triangulation from point cloud to show the topological information of a model. The related point cloud processing techniques are summarized in the following Figure 2.1.

To analyze shape characters of 3D model, the geometric features should be extracted by estimating some basic values [12], for example, normal vector and curvature of points [59]. Based on these values, shape descriptors [33] are constructed to represent 3D local shape feature. With the features, a variety of research can be studied.

**Single model.** Simplification reduces the amount of acquired point data to save the storage capacity and the processing time [48]. Down-sampling [39], one of resampling, is a similar notion with simplification. The other relative notion is up-sampling. segmentation [66] is to cluster points with similar characteristics into homogeneous regions, it allows that an interest region is

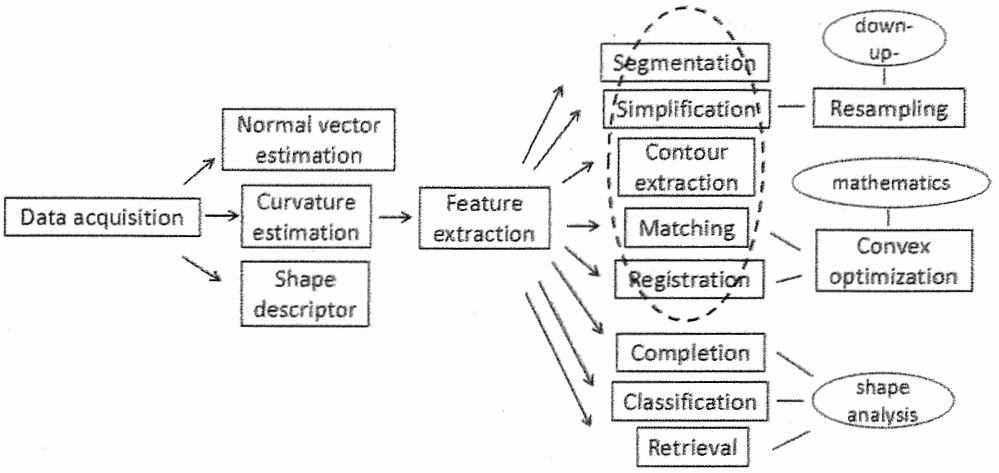


Figure 2.1: Point Cloud Techniques. Techniques that applied on our research are marked in the cycle.

extracted from the whole point cloud.

**Multiple models.** Registration is a problem of consistently aligning various overlapping 3D point cloud data views into a complete model in a rigid sense [78]. Matching is frequently used to describe the problem of reassembling fragments [69]. In mathematics, matching and registration can be regarded as the convex optimization problem [18]. Furthermore, Object completion [57] and composition [38] can create non-existent parts of models.

**Massive models.** 3D shape classification is important for browsing, managing and organizing large 3D shape collections [87]. Content-based shape retrieval techniques can facilitate 3D model resource reuse, 3D model modeling, object recognition, and 3D content classification [52].

In archaeology, lithic artifacts [44] are studied by measurement and shape analysis [65, 86]. Currently, 3D technology has applied on documentation and typology of lithic artifacts [32], and provided an alternative to instead of lithic illustration [53]. Shott [85] surveyed the challenges and prospects for analysis of digital models of stone tools. Sumner et al. [89] reviewed a cost-effective, photogrammetric-based three-dimensional modeling system that utilizes digital artifact images and commercial software. Porter et al. [73] developed a photography rig for the express purpose of systematically capturing images for the creation of 3D photogrammetric models. Lin et al. [51] reported on the use of a 3D laser scanner to obtain precise measurements from experimen-

tal lithic reduction sets. Wickeroth et al. [95] presented a new free software tool called ArtefactViewer tailored specifically to the needs of archeologists working with data from 3D scans. Willis [96] discussed the state-of-the-art in computational analysis and reconstruction of archaeological ceramic vessels. Park [70] introduces a method to measure the average shape of handaxes, and characterize deviations from this average shape by taking into account both internal and external information. Riddle and Chazan [75] outlined a new method for quantifying distribution of mass in lithic specimens from three-dimensional point-cloud data. Richardson [74] proposed a method for automatic, objective and precise documentation of the tool surface, together with a quantitative analysis of the scar and the ridge networks. Bretzke and Conard [19] presented a method to quantify morphological variability in lithic artifacts using 3D models of stone artifacts. Clarkson et al. [27] developed a mathematical formula for describing scar patterning using vectors calculated from the start and end points of flake scars recorded in three dimensions.

Digital technologies are also transforming the way cultural heritage researchers, archaeologists, and curators work by providing new ways to collaborate, record excavations, and restore artifacts[83]. [81] presented a few recent experiences where high-quality 3D models have been used in CH research, restoration, and conservation. [31] surveyed the state-of-the-art approaches and challenges of 3D reconstruction methods for digital preservation of cultural heritage. [13] described how some innovative methodologies have been designed and employed to support the restoration of a fragmented terracotta statue. Serious games are used for learning cultural heritage, [62] provided the state-of-the-art of serious games in this domain and analyzed the complex relations between genre, context of use, technological solutions and learning effectiveness.

## 2.2 Previous Works

### 2.2.1 Data Acquisition

Our data are acquired from a 3D surface reconstruction technique using four-directional measurement machine developed by Iwate University and LANG Co., Ltd. [10, 24]. Hundreds of stone tools can be scanned at the same time

and the surface feature is intact preserved, such as sharp edges, flake scars, benefiting from the highest 0.1 *mm* precision of laser scanner. Additionally, the stone tools are from archaeological researchers in the university and the Buried Cultural Property Investigation Center which we cooperated with. In the actual data, there are some holes need to be filled manually, and some data are not registered very well.

Figure 2.2: Scanning Device.

### 2.2.2 Simplification

A new point cloud simplification method [102] is proposed that can maintain the characteristics of surface shape for unstructured point clouds. In this method, a segmentation range based on mean curvature of point cloud can be controlled. The simplification process is completed by maintaining the position of the representative point and removing the represented points using the range. Our method can simplify results with highly simplified rate with preserving the form feature. Applying the proposed method to 3D stone tool models, the method is evaluated precisely and effectively.

Figure 2.3 shows three stone tool models simplified by using the proposed method. The number of points of No.L0197A0178 model was reduced to 3.73% of those in its original model. In the right column of Figure 2.3, the preserved points of models were clearly shown by surfels(surface elements proposed in

L0197A0178 ($\alpha = 0.9$)

Figure 2.3: Simplified results of the new method. Left: original point clouds(triangulated); middle: simplified point clouds(triangulated); right: simplified point clouds(surfel[71])

[71]). The experimental results indicate that the new method can maintain the boundaries and ridges of 3D models. The evaluation results of the maximum normalized distance indicate that the error between simplified result and the original point cloud is very small, and the simplified results are more than adequate requirements of matching study [26]; that is, the new simplification method has a good effect on the pre-processing of the matching study. The limitation of this method is it not easy to control the point density of simplified point cloud.

### 2.2.3 Matching

For matching research, Yamahara et al. [99] proposed a method for pairwise matching of lithic refitting materials. Sato et al. [80] proposed a flake surface reconstruction method to make flake matching more efficiency. Then, based on these works, Chida et al. [26] studied on a method to search adjacent

flake surfaces on stone implements for generating a joining material. In their method, the segmentation and simplification struggle with good results of flake surface, therefore several groups mixed lithic materials cannot be processed together. Additionally, they did not finish a complete system, thus some software or tools have to be used to help with matching work.

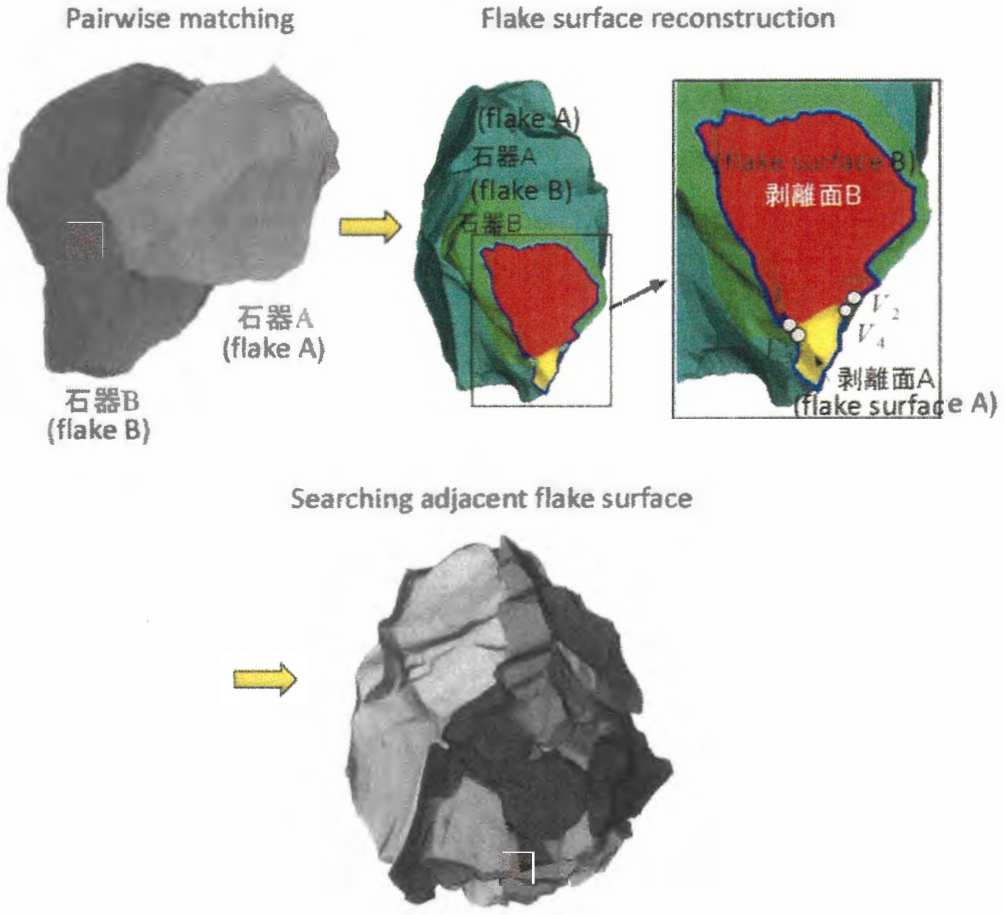


Figure 2.4: Previous works about matching.

# Chapter 3

# Matching

## 3.1 Overview

This chapter introduces the related works of matching and registration and the properties of flake surface, and explain the problems of related works when applied to lithic materials. With improving the previous method, a new pipeline to matching mixture lithic refitting materials is proposed. However, this method still has a limitation. Therefore, a new algorithm based on point cloud is developed to solve this limitation.

## 3.2 Related Works

### 3.2.1 Matching and Registration

In point-cloud-based techniques, registration methods work to merge several data points obtained from different perspectives under a single model. In contrast, matching methods work to restore fragments according to multiple models. Nevertheless, the core algorithms of both approaches are extremely similar.

The most widely applied methods are Iterative Closest Point (ICP) [16, 77] and Random Sample Consensus (RANSAC) [22]. The defects of ICP are that correct correspondence is dependent on a satisfactory initial pose [76], and the matching of partial overlap does not work well. On the other hand,

RANSAC is a robust method for managing partial overlaps; however, it has poor efficiency. Many researchers have proposed improved ICP [23, 105] and RANSAC [9, 58] methods. For example, the S-ICP [17, 56] is introduced to solve practical implementation problems. Then, the Go-ICP [100] is presented to study a globally optimal algorithm for solving the initialization problem. In this study, the proposed matching method is developed by enhancing the RANSAC algorithm to also accommodate flake models.

Many descriptors based on feature matching have been studied. The basic approach is to first extract the feature points and calculate the descriptor for each point, and then to establish point-to-point correspondences by matching the evaluated descriptors. Guo et al. [33] have conducted a detailed comparisons of a number of 3D local feature descriptors based on descriptiveness and robustness. For instance, Fast Point Feature Histograms (FPFH) [78] and Signature of Histograms of Orientations (SHOT) [79] achieve good performance in terms of both feature matching accuracy and computational efficiency, for point clouds with a small and a large number of points, respectively. Further, Rotational Projection Statistics (RoPS) [34] is the best option when the characteristics of a dataset are unknown, as this technique consistently produces good results on different datasets. Intrinsic Shape Signatures with Boundary Point Removal (ISS-BR) [106] yields the best performance when combined with 3D key-point detection methods. Tri-Spin-Image (TriSI) [35], Unique Shape Context (USC) [94], and 3DSC [28] have the best scalability with respect to an increasing number of models. Note that TriSI is the best choice for applications on large datasets, as the computational and storage costs of both USC and 3DSC are high.

Moreover, Huang [40] et al. presented a system with good performance for automatic reassembly of broken 3D solids. Winkelbach and Wahl [97] proposed an efficient surface matching approach for reassembling broken solids using cluster trees. In addition, Altantsetseg [11] et al. introduced a new descriptor that contains both feature points and curves for pairwise matching of broken fragments using Fast Fourier Transform (FFT). Song and Chen [88] developed a local voxelizer descriptor for surface registration that is constructed using a unique Local Reference Frame (LRF). Furthermore, Yang et al. [101] proposed a local feature statistics histogram (LFSH) for 3D point cloud registration. For flake models, however, the low curvature variation of the flake

surface and the uniform point distribution blur the descriptor recognition and correspondence.

With regard to culture heritage applications, a previous survey [72] summarized a large number of analytical techniques implemented on the micro-, meso-, and macro-scale. In addition, the contour-line-based method has also been applied to 2D fragments [6, 46] and Fresco fragments [15, 20, 30, 93].

Various matching methods have been developed in the past, for application to archaeological fragments or other types of data. However, a few algorithms have yielded satisfactory experimental results when applied to flakes. Brown et al. [20] presented a system for matching fresco fragments to reassemble Theran wall paintings. This method requires feature extraction of surface curvature, whereas the flake surfaces of lithic materials are almost flat and smooth and the features that can be extracted are very limited. Huang et al. [40] presented a system with good performance for automatic reassembly of broken 3D solids. It is an excellent reference, but it is not entirely suitable for our research because the refitting of lithic materials has some unique principles [42], whose details are described in Section 3.3.3. The reasons can be summed up as follows: (1) Global matching algorithms yield unsatisfactory results, since a pair of flake surfaces require partial matching; (2) Descriptor-based methods struggle to extract features, because flake surfaces have less obvious regional features.

In the previous work, Chida et al. [26] proposed a rapid searching method of adjacent flake surfaces for lithic materials. The paper [26] does not detail the simplification status, while their simplification could not obtain simplified results with the roughly same simplified standard for mixture lithic materials. Therefore, the matching method could not obtain good results with unified parameters for the mixture lithic materials. In addition, this method limited the search ranges of matching flake surface, while the search ranges are ambiguous for difference groups of lithic materials. In their mixture experiment, their method can obtain 83% correct results with top five flakes by D2, and 94% correct results with top ten. Therefore, this paper presents a new method that is suitable for stone-tool flake matching.

### 3.2.2 Flake Surfaces

Flake surfaces are fractures produced by peeling a stone into flakes. For example, Figure 3.1 (a) shows the flake surfaces of flakes $A$ and $B$ segmented by blue boundary lines. Flakes $A$ and $B$ can be matched into one flake as shown in Figure 3.1 (b), because the two corresponding flake surfaces $F_A$ and $F_B$ are produced at the same time. Therefore, flake surface matching is studied to solve the refitting issue of lithic materials. However, the previous method [26] only can solve the problems of pairwise matching or refitting lithic materials from a single stone core. With improving the previous methods, we improve the method [26] for refitting mixture lithic materials from multiple groups.

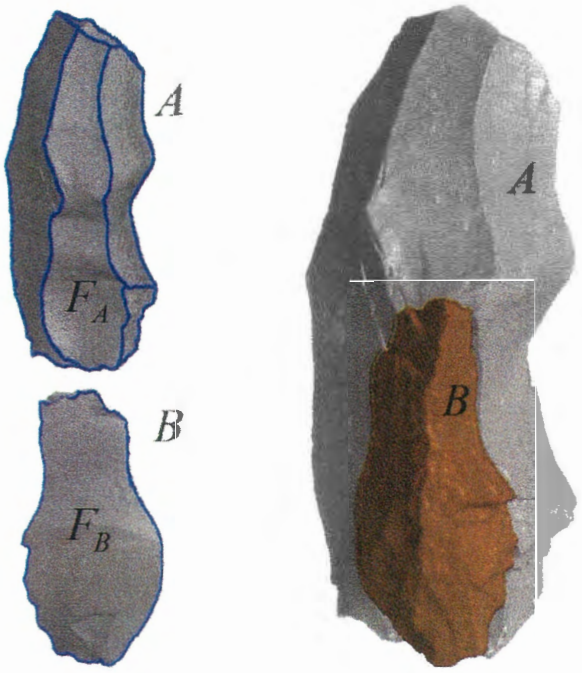


Figure 3.1: Matching by flake surfaces.

## 3.3 Matching Based on Mesh

### 3.3.1 Algorithm Overview

The input to our algorithm is a set of stone tool point clouds measured by [10]. Based on the pipeline of the method [26], we improve their algorithm for mixture lithic materials. The algorithm is executed in the following procedure:

1. Each point cloud is segmented for obtaining flake surfaces. Automatic segmentation is applied in place of the semi-automatic method.

2. Each flake surface is simplified to reduce the number of point cloud. New simplification is employed based on point clouds that can control simplified flake surfaces via the same evaluation with the matching method. The input flake surfaces are improved by the new segmentation and simplification, and a premise is provided for refitting mixture lithic materials with the same threshold parameter.

3. From each flake surface of stone cores, the matching algorithm is used to search the best matching surface and the transform matrix is computed. For the mixture lithic materials, all flake surfaces instead of partial ones are computed until find the best matching surface is found with the D2 order.

4. All flake surfaces belonging to one stone tool with the matched surface are transformed by the matrix.

5. The new flake surfaces of the matched stone tools are reconstructed.

6. The matching process is repeated until all stone tools are matched.

Thus, point clouds of all lithic materials are refitted by the transform matrices.

### 3.3.2 Segmentation and Simplification of Flake Surfaces

In our method, the algorithm of region growing segmentation [84] is applied to obtain flake surfaces. The two parameters, angle threshold of normal vector $\theta$ and curvature threshold $c$, are used to get a superb segmentation result. The

greater values of $\theta$ and $c$ lead to the smaller number of flake surfaces. The gravel surfaces (that belong to the original rock, not to a flake surface) and the flake surfaces whose number of points is smaller than 1/20 of the original points are removed. They are not put into flake surfaces that will be matched.

Matching of the original point clouds requires a large amount of computing time due to the large number of points, which makes the simplification process necessary. The point cloud simplification [102] based on curvature is employed to simplify the flake surfaces that described in Section 2.2.2. Matching will fail if the features of adjacent flake surfaces are changed by simplification. While, in this method, the features can be maintained by comparing with the original shapes. Parameter $\alpha$ of the distance threshold is set to control the number of simplified points, and the greater $\alpha$ leads to the smaller number of simplified points. Furthermore, the successful rate of mixture matching is raised because the same evaluation as matching process is applied in this simplification. In this paper, the algorithm of fast triangulation [3, 54] is applied to reconstructed polygon meshes for simplified flake surfaces. The polygon meshes will be used to evaluate simplification result and matching process.

### 3.3.3 Mixture Matching

In our previous research [26], it was extremely difficult to control every flake surface in the same simplified degree with other simplification algorithm, and this led to large simplified differences among the groups. Thus, matching method described in [26] cannot be applied for mixture lithic materials. While the simplification method [102] in this research can obtain simplification results in the same evaluation value for all flake surfaces, the minimal simplified errors are maintained between the original point clouds and the simplified ones by computing the same normalized distance as matching evaluation. Depending on favorable segmentation and simplification results, lithic materials can be refitted with mixture materials of several groups at once.

Additionally, there are three properties to make lithic material refitting different from other fractured object reassembling, as shown in Figure 3.2. The first property is that there is a time difference in generation of multiple flakes from a single core [42]. In other words, lithic material refitting is not an operation to match two flakes arbitrarily. It must follow an order. Suppose

flake $A$ is peeled first and then flake $B$ is peeled, as an example. In the viewpoint that the flakes are peeled from a rock one by one and the rest is the stone core, the flakes should be matched with the stone core in reverse order. The second property is that most of flake surfaces used for matching are flat and smooth since the selected stone can be divided sharply [55]. According to this property, it is not suitable to use the general matching algorithm based on surface features. The third property is that one flake surface may be divided into several pieces. For example, in order to match flake $A$, flake $B$ should be matched with the core to get flake surface $F_C$ by combining flake surfaces $F_1$ and $F_2$. Thus, the matched flake surfaces must be reconstructed to search the next surface.

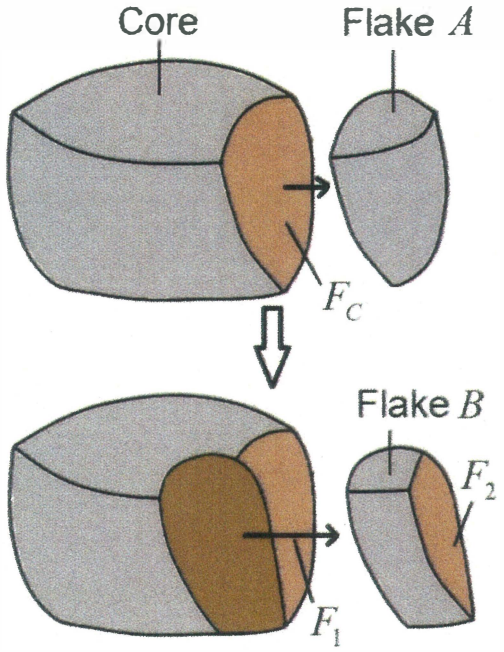


Figure 3.2: A case of making a stone tool (flake $A$ is peeled first and flake $B$ next).

In our method, the stone cores are specified manually and the matching process begins on flake surfaces of a stone core. As the data is mixed with multiple stone cores in our research, the stone cores are refitted in succession. Each flake surface of a core is matched with each flake surface of flakes to search the best matching flake surface later. In order to reduce the number

of tasks for matching, shape distribution D2 [67] of each flake surface is computed, and the matching order is sorted by the Manhattan Distance of each pair. Figure 3.3 shows the result of D2 distribution computation for four different flake surfaces by a spot chart. The black, red, blue and green points show the D2 shape distribution of meshed flake surfaces 1, 2, 3 and 4 respectively. We can see the shape of flake surface 1 is similar to 2, and different from 3 and 4. The difference between flake surfaces 1 and 2 is significantly less than the difference between 1 and 3 or 4. Therefore, the sorted matching order could improve the efficiency of our matching process.

Normalized distance $D$ [99] is applied for finding the best matching flake surfaces. It provides a standard to measure the difference between two flake surfaces on a unit area. Normalized distance $D$ of each pair is calculated as equations (3.1) and (3.2), and the best matching flake surface is judged by a value smaller than threshold parameter $d$. Figure 3.4 shows the computing method of normalized distance. In the equations and Figure 3.4, $\mathbf{V}_i$ is a point on flake surface $A$, $T_i$ is the triangle on flake surface $B$ closest to $\mathbf{V}_i$ , $\mathbf{n}_i$ is the normal vector of $T_i$ and $\mathbf{g}_i$ is the geometric center of $T_i$. Then distance $d_i$ between $\mathbf{V}_i$ and $T_i$ can be calculated by equation (3.1). $D$ is computed by the sum of $(d_i)^2$, dividing mesh area $S$ of flake surface $B$ like equation (3.2).

$$d_i = (\mathbf{V}_i - \mathbf{g}_i) \cdot \mathbf{n}_i \tag{3.1}$$

$$D = \frac{1}{S} \sum_{i=1}^{n} (d_i)^2 \tag{3.2}$$

Our pairwise matching algorithm is proposed in the following steps and Figure 3.5:

1. Set a polygon mesh with the smaller area as source mesh $F_s$, and the one with the larger area as target mesh $F_t$.

2. For meshes $F_s$ and $F_t$, search their edge line sets $E_s$ and $E_t$ and edge triangle sets $T_s$ and $T_t$. For each pair of $E_{si}$ and $E_{tj}$, obtain vectors $V_{si}$ and $V_{tj}$ in counterclockwise direction for normal vectors $N_{si}$ and $N_{tj}$ of triangles $T_{si}$ and $T_{tj}$.

3. Construct local coordinate systems $S_{si}$ and $S_{tj}$. For $S_{si}$, set the direction of edge vector $V_{si}$ to the $x$ axis, that of normal vector $N_{si}$ to the $y$ axis, and that of $V_{si} \times N_{si}$ to the $z$ axis. Then, match local coordinate system

$S_{si}$ to $S_{tj}$ and compute transform matrix $M_a$. In addition, transform $F_s$ with $M_a$ to get $F_s\prime$.

4. Search the nearest triangle in $F_t$ for each triangle of $F_s\prime$ by their barycenter. Calculate the sum of distances between each barycenter pair $d_c$. Select $F_s\prime$ with the minimum value of $d_c$. Search the nearest triangle $T_i$ from $F_t$ for each point $P_i$ from $F_s\prime$. Get point $P_i\prime$ by projecting $P_i$ in $T_i$ and construct point set $P\prime$.

5. Calculate fitting transform matrix $M_b$ by matching point set $P$ of $F_s\prime$ to $P\prime$.

6. Finally, matching transform matrix $M$ is computed by $M_a \times M_b$.

Thus, the source flake could be matched with the target flake by transform matrix $M$.

### 3.3.4 Flake Surface Reconstruction

In order to reconstruct the original flake surface, the divided flake surfaces should be detected and made into one flake surface after matching two flakes. Figure 3.6 shows the reconstruction of flake surfaces $F_a$ and $F_b$, where the two matched flake surfaces are shown in darker gray. The flake surfaces are reconstructed in the following procedure:

1. For each pair of flake surface $F_a$ and $F_b$ of two matched flake surfaces sets, search nearest point $P_{bj}$ from $F_b$ for each point $P_{ai}$ from $F_a$. If the distance between $P_{ai}$ and $P_{bj}$ is shorter than distance threshold $d_r$, they are put into the corresponding point pair set $P_c$.

2. For each point in $P_c$, search the triangles that belong to the point. For point $P_{ai}$ on $F_a$, triangle set $T_{ai}$ on $F_a$ can be obtained. Then, compute mean vector $V_{ai}$ from all normal vectors of the triangles in $T_{ai}$.

3. Calculate the angle between each vector pair $V_{ai}$ and $V_{bi}$. If both angles are smaller than angle threshold $\theta_r$, the flake surface pair $F_a$ and $F_b$ should be reconstructed to one flake surface.

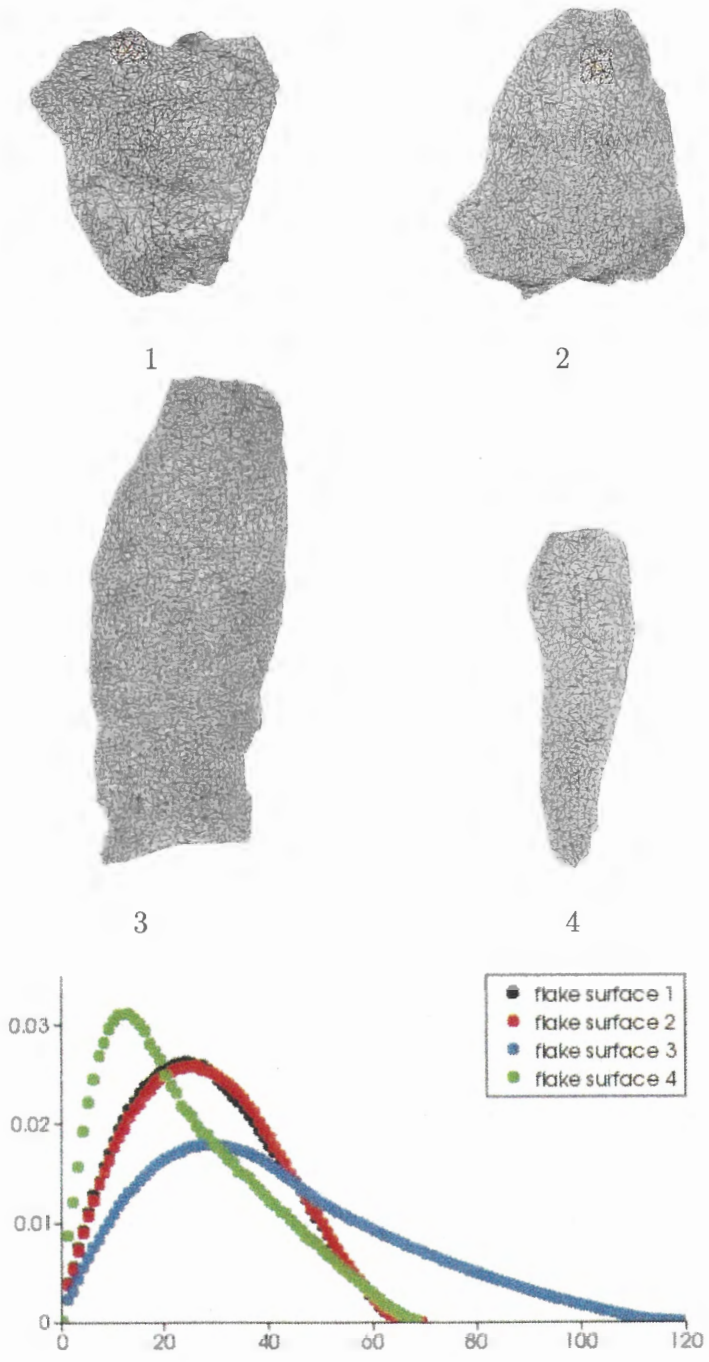


Figure 3.3: D2 distribution on four flake surfaces.

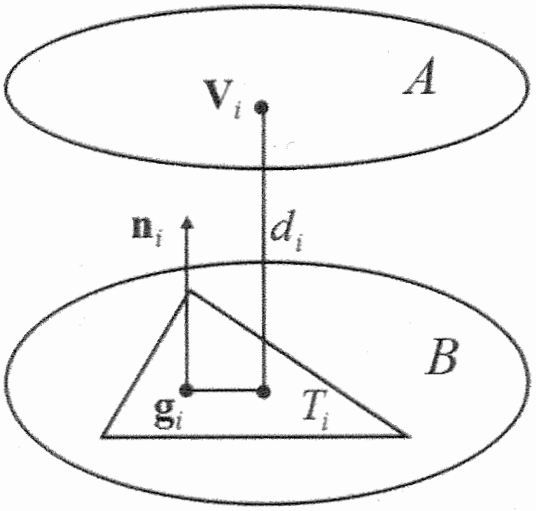


Figure 3.4: Computing method of normalized distance.

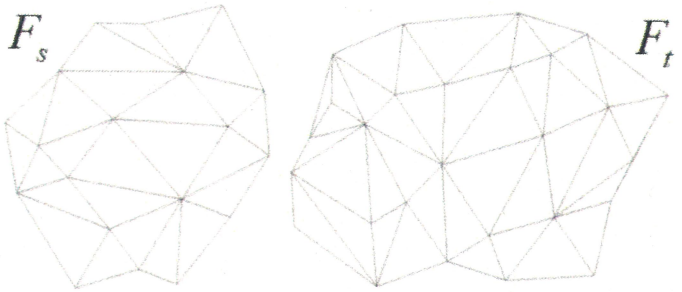


(a)

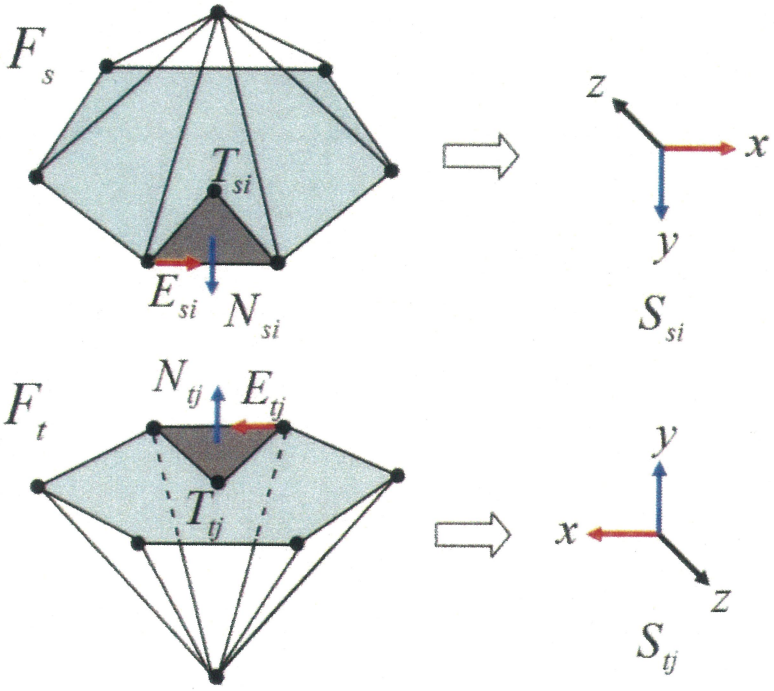


(b)

Figure 3.5: Matching algorithm.

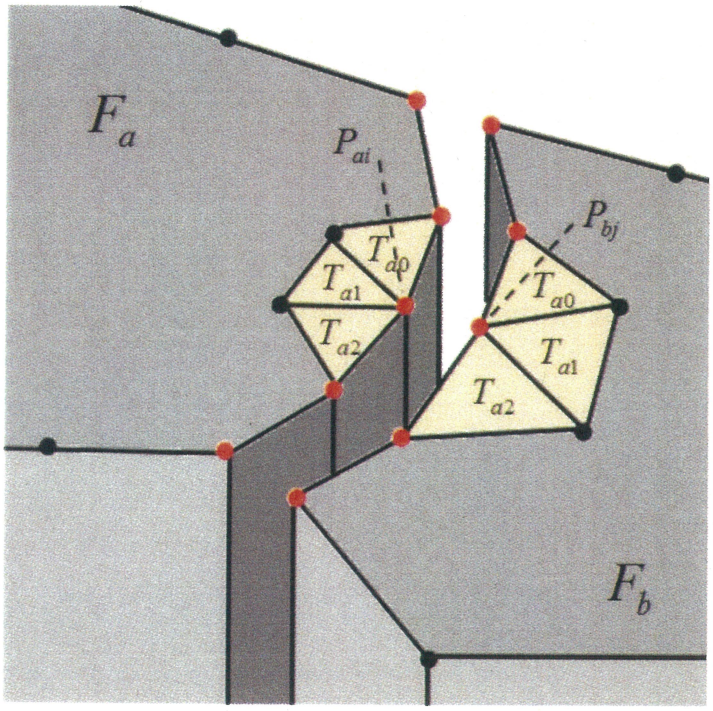


Figure 3.6: Searching reconstruction flake surfaces.

### 3.3.5 Experimental Results

We have implemented the new method using C++ and PCL [4], and examined the method in a PC with Intel Core i7-4790 CPU and 8.00GB memory. The data of 43 lithic material imitations were examined in our experiment, shown in Figure 3.7. *No.*01 and *No.*20 shown with black thick frames are the stone cores. The 43 data could be refitted into two groups by our new matching algorithm in the order of *No.*01 and *No.*20.

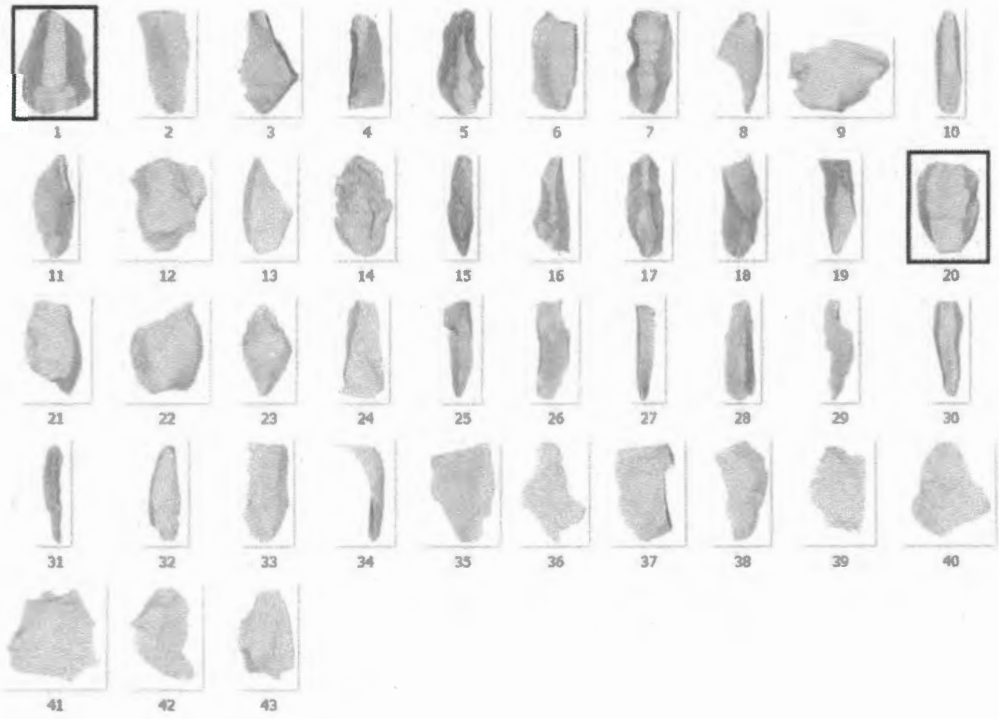


Figure 3.7: 43 experiment data.

Figure 3.8 shows the segmentation results of *No.*13 by point clouds. The flake surfaces are displayed in different colors. The red points do not belong to any flake surfaces. There are about 833 thousand points, the execution times are about 95 seconds, and four flake surfaces are segmented for matching. From this figure, we can clearly see that the flake surfaces of stone tool models are segmented precisely and integrated.

Figure 3.9 shows the constructed meshes and faces of three simplified flake surfaces of *No.*13. Distance threshold parameter $\alpha$ is set to 3.0. For the three flake surfaces from left to right, the number of the original point clouds,

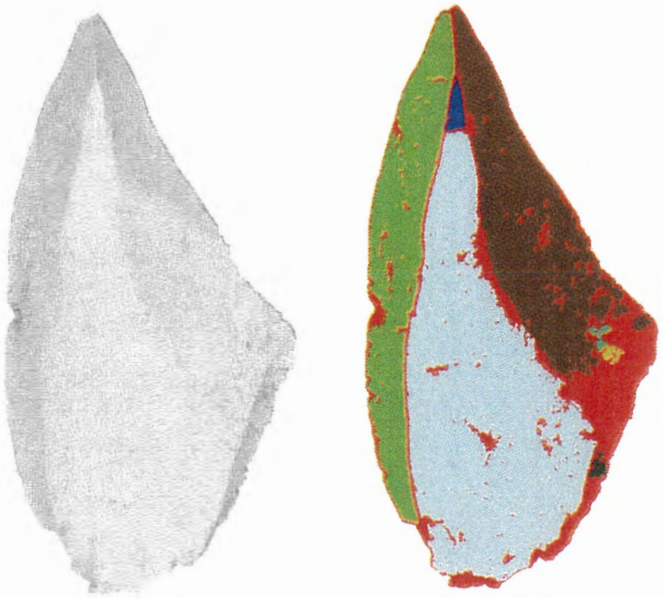

*No.*13 ($\theta = 1.5$, $c = 1.0$)

Figure 3.8: Results of segmentation.

the number of the simplified point clouds, simplified rate, execution times and normalized distance are shown in the Table 3.1. The number of the original point clouds are 78119, 167834 and 86643 and the number of the simplified point clouds are 591, 1095 and 628. The numbers of points are reduced to 0.76%, 0.65% and 0.72%. The execution times are about 4.4, 11.5, and 5.8 seconds. The normalized distance is employed to evaluate the result of simplification, and their normalized distances are about 0.090, 0.066 and 0.067. The normalized distances show that the simplified results are very close to the original point clouds, and we can see that the contour lines are almost identical. Thus, the simplified flake surfaces can be used for matching very well. Furthermore, the simplified process can drastically reduce the computing time of matching.

Through the process of segmentation and simplification, the 43 data are divided into 169 flake surfaces for mixture matching algorithm. Figure 3.10 shows the result of pairwise matching of two stone tools *No.*1 and *No.*7. Figure 3.11 shows a case of matching where some matched flake surfaces must be reconstructed into one flake surface to match with the next one. Three flake surfaces of stone tools *No.*8, *No.*13 and *No.*18 are reconstructed to match with

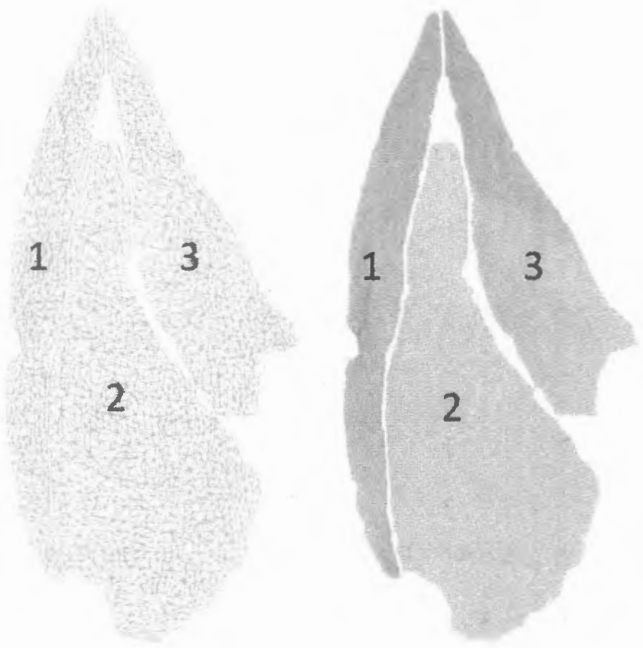


(a) Mesh (b) Face

Figure 3.9: Results of Simplification.

*No.*19.

Tables 3.2 and 3.3 show the details of matching groups 1 and 2. In the tables, *Number* indicates the flake surfaces matched currently, where the digits are the number of stone tools, and the alphabets are the number of flake surfaces produced from the same stone tool. *Order* indicates the sorted order of flake surfaces for searching the best matching flake surface by D2. Long execution time is required for calculating the fitting transform matrix for each pair, and a large number of pairs need to be computed. For example, the execution time is 1007.9 seconds for searching the best matching flake surface $06A$ in the group 1. The average matching time is about 32.5 seconds for each pair, while 31 times of matching are required. All flake surfaces are matched starting from the two stone cores *No.*01 and *No.*20. The threshold parameter of normalized distance $d$ is set to 0.06 to judge the best matching flake surface. Finally, sixteen stone tools are matched in group 1, and twelve are matched in group 2. Flake $E$ cannot be matched by our method, and the details are described in Section 3.3.6. Figure 3.12 and Figure 3.13 show the results of the final matching for groups 1 and 2 and the pictures of imitations

Table 3.1: Results of Simplification.

| Flake | 1 | 2 | 3 |
|---|---|---|---|
| Original number | 78119 | 167834 | 86643 |
| Simplified number | 591 | 1095 | 628 |
| Simplified rate | 0.76% | 0.65% | 0.72% |
| Execution time | 4.4s | 11.5s | 5.8s |
| Normalized distance | 0.090 | 0.066 | 0.067 |

matched by hands.

Table 3.2: Matching of group 1.

| Number | Order | Normalized distance | Time |
|---|---|---|---|
| 01$A$-12$B$ | 1/163 | 0.0248339 | 121.0s |
| └06$A$ | 31/160 | 0.0565872 | 1007.9s |
| └10$B$ | 45/156 | 0.0253672 | 1758.9s |
| └07$B$ | 1/152 | 0.0429291 | 88.6s |
| ... | ... | ... | ... |
| └04$B$ | 45/113 | 0.0148311 | 140.3s |
| Total | 15846.5s | | |

### 3.3.6 Limitation

Figure 3.14 shows an example where our method cannot match. The two red circles show the corresponding points of matching. The two flake surfaces overlap partially (shown by the gray diagonal lines), and the one with the larger area shown in the right cannot be completely cover the other. Because of this, the minimum distance of the two flake surfaces could not be computed correctly. Our method results in an error for such flake surfaces. The incidence

Table 3.3: Matching of group 2.

| Number | Order | Normalized distance | Time |
|---|---|---|---|
| 21$A$-25$D$ | 30/99 | 0.0348425 | 992.8s |
| └34$A$ | 3/94 | 0.0071474 | 19.5s |
| └33$A$ | 7/91 | 0.0219804 | 47.6s |
| └07$E$ | 7/86 | 0.0580872 | 376.2s |
| ... | ... | ... | ... |
| └35$D$ | 4/59 | 0.0130739 | 142.9s |
| Total | 4399.5s | | |

rate of such case depends on the condition of lithic materials, and there is only one in this experiment.

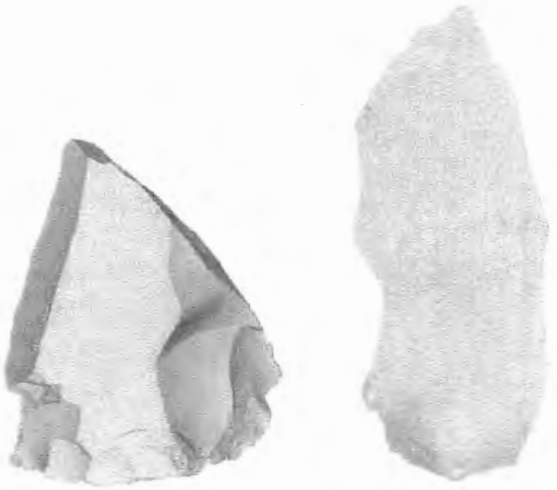

(a) *No.*1 (b) *No.*7

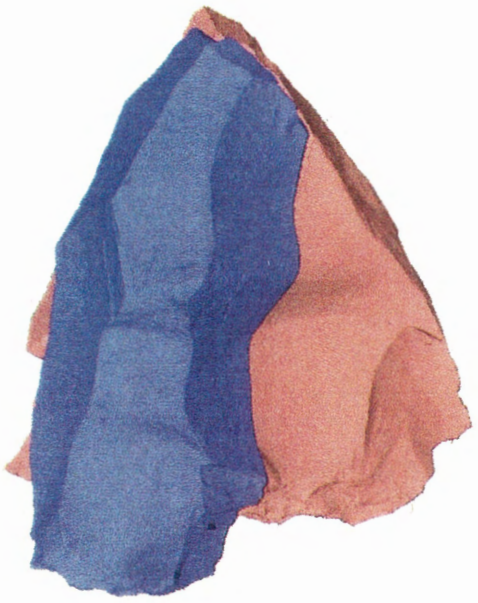

(c) Result of matching

Figure 3.10: Result of pairwise matching.

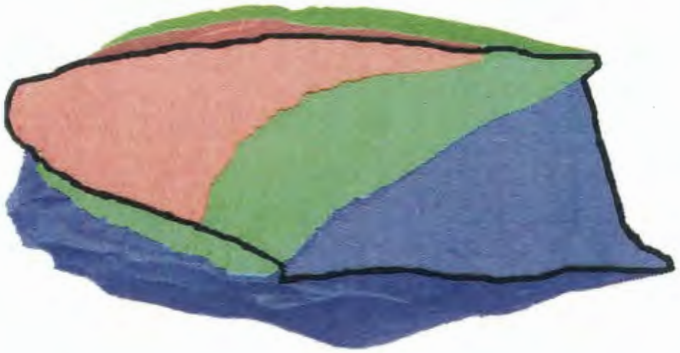

(a) Reconstructed flake surfaces of *No.*8, *No.*13 and *No.*18.

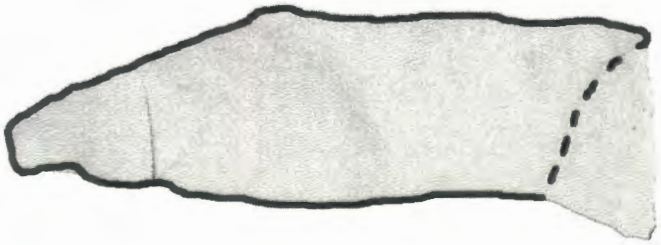

(b) Target flake *No.*19.

(c) Result of matching.

Figure 3.11: Result of reconstruction.

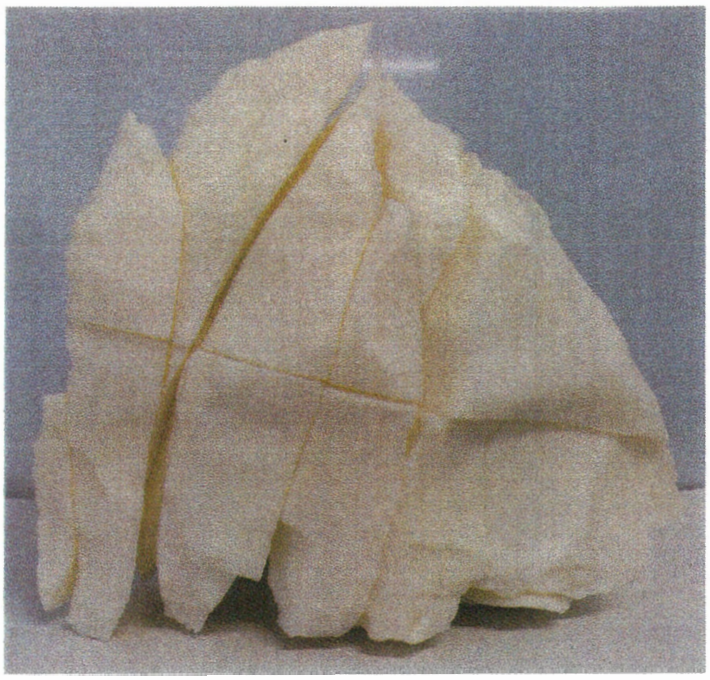

(a) Matched flakes of group 1.

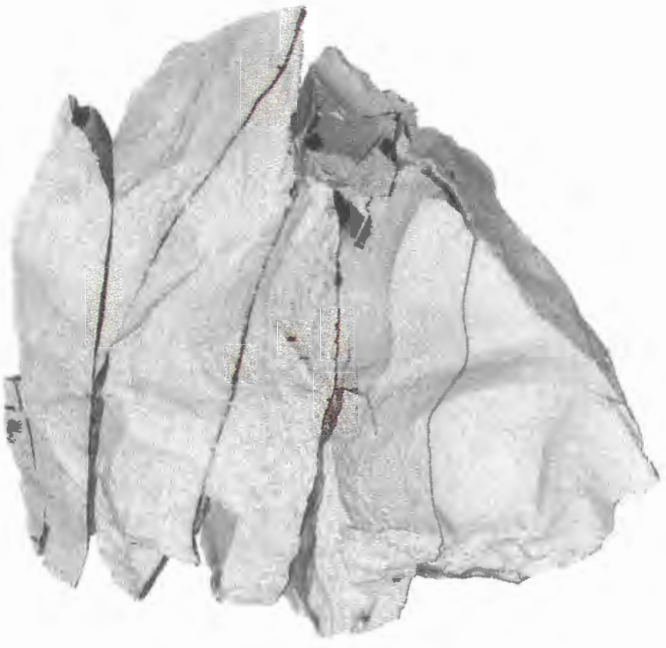

(c) Group 1 matched by our new method.

Figure 3.12: An actual picture and the result of final matching for group 1.

(a) Matched flakes of group 2.

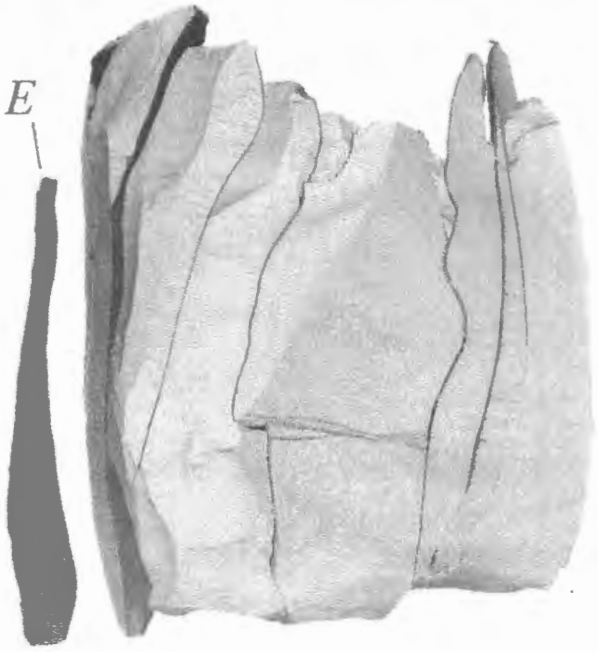


(b) Group 2 matched by our new method.

Figure 3.13: An actual picture and the result of final matching for group 2.

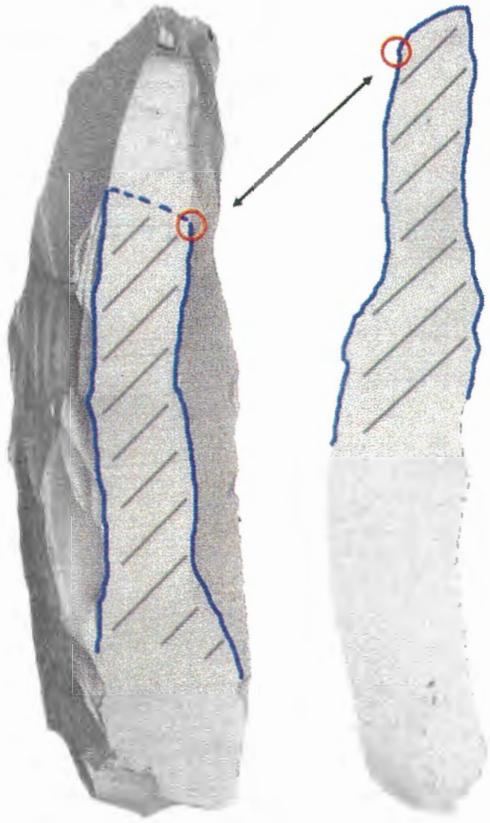

Figure 3.14: Limitation of our method..

## 3.4 Matching Based on Point Cloud

### 3.4.1 Overview

By analyzing flake matching scenarios, we observed that each flake pair was always matched as part of a contour line, regardless of whether partial or full overlap of the flake surfaces occurred. Consequently, we developed a new method based on contour points and normal vectors for pairwise matching of flakes. The input of our method is a pair of flake models from the point cloud. First, the normal vectors are calculated for each point. Second, each flake surface is segmented and uniformly downsampled; then, the contour points are extracted. Finally, the flake surface pair with the best matching is rapidly identified based on the contour points, and further matching is conducted using the nearest point sets.

### 3.4.2 Preparation Work

The preparation work of our method includes flake surface segmentation and contour point extraction for each flake, as shown in Figure 3.15. First, the normal vectors of the points are calculated via a least-square plane fitting estimation. The consistency and outward directions of the normal vectors should be ensured. Then, a standard region growing algorithm is implemented on the flake to yield a set of flake surfaces. A flake, most likely possesses flake surfaces only, or has both flake surfaces and gravel faces. The flake surface is an almost flat or smooth surface that constitutes the fracture surface between two flakes. The gravel surfaces are intensely rough, because they correspond to the surface of the original rock. In our method, the gravel surfaces are divided into many trivial clusters, which are not used for matching.

To enhance the matching efficiency, the point numbers of the flake surface are reduced using the uniform downsampling algorithm. The sampling interval determines the efficiency and accuracy of the coarse matching. Then, the contour points are extracted using the convex hull algorithm. It is important to note here that the contour points are sorted in the counter-clockwise direction along the normal vector of the surface, to facilitate contour interception. In brief, one flake surface contains three point-set elements: the original $\{Op\}$, sampling $\{Sp\}$, and contour $\{Cp\}$ point sets.

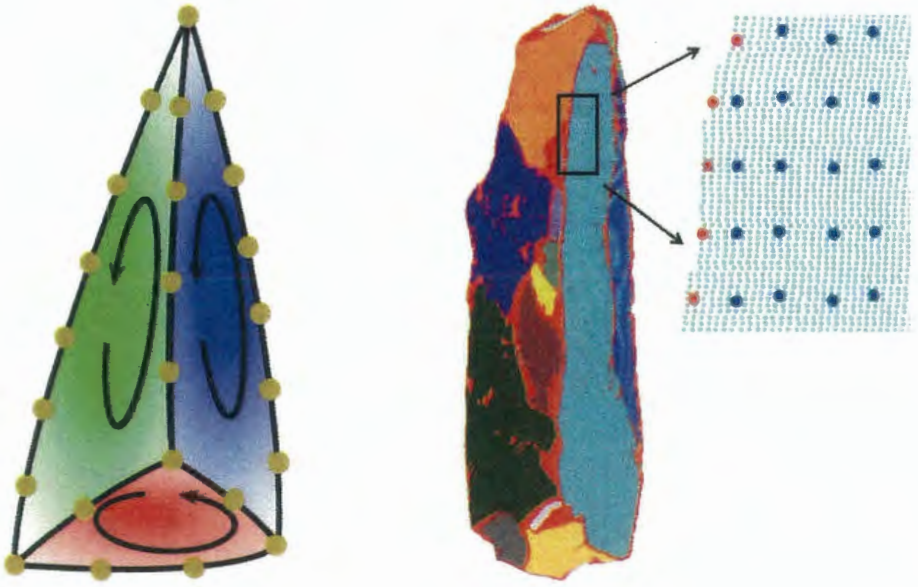

(a) (b)

Figure 3.15: Segmenting flake surfaces from a single flake. (a) The concept model is segmented into several surfaces indicated by different colors. The circular arrows show the ordering directions of the contour points. (b) An actual flake is segmented into several flake surfaces, where one color represents one flake surface. In the enlarged detail, the original, sampling, and contour points are shown in cyan, blue, and red, respectively.

### 3.4.3 Pairwise Matching

A coarse-to-fine method is applied to all flake surface pairs for pairwise rigid registration. The surface with a smaller point number is set as the source surface $S$, while the one with the larger point number is set as the target surface $T$. Two 4-point sets $\{p_{i-n}, p_i, p_{i+n}, p_v\}$ and $\{p'_{i+n}, p'_i, p'_{i-n}, p'_v\}$ are constructed based on the contour points to compute the coarse rigid transform matrix $M_a$, which aligns $S$ to $T$, as shown in Figure 3.16. The point $p_i$ is a contour point on $S$ and the two points $p_{i-n}$ and $p_{i+n}$ are separated from $p_i$ by $n$. The normal vector $v_i$ of point $p_i$ is computed from the mean value of all the normal vectors of the points in the range $r$ of $p_i$. The point $p_v$ is on $v_i$, with distance $r$ from $p_i$. Similarly, the first three points are constructed in the same manner on the target surface, whereas the point $p'_v$ must be on the

reverse extension line of $v_i'$. There are two reasons for the construction of the fourth point: (1) The two mean normal vectors $v_i$ and $v_i'$ represent the match of a partial edge region pair between two surfaces; (2) The fourth point is not on the same plane as the first three points.

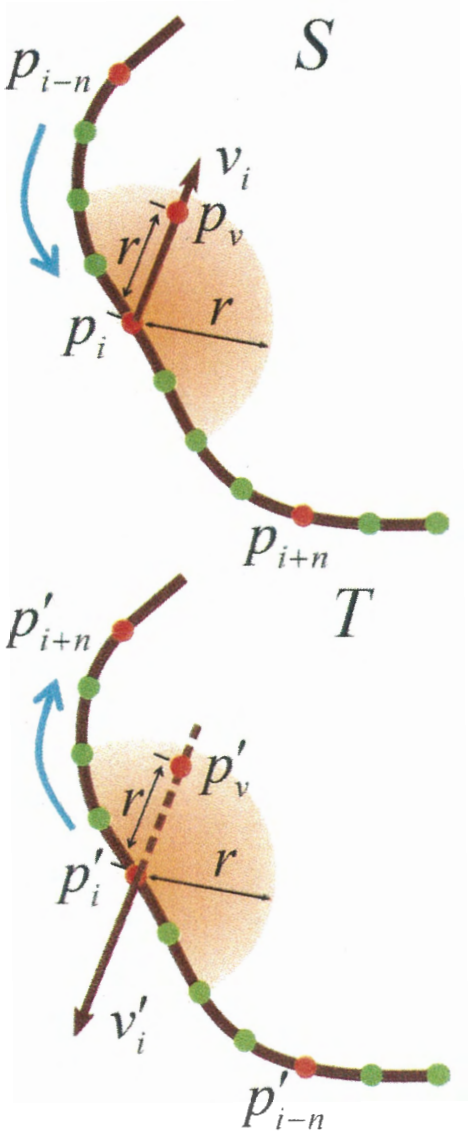


Figure 3.16: Construction of 4 points for source $S$ and target $T$ surfaces.

The point set $\{p\} \in \{Cp\}$ between $p_{i-n}$ and $p_{i+n}$ is transformed by $M_a$ to measure the difference from $\{p'\}$. To improve the robustness of the error metric, point-to-region distances are employed instead of point-to-point dis-

tances. as shown in Figure 3.17. Furthermore, the error is computed using equation (3.3). We assume that two points are matched when the distance is smaller than $\frac{\sqrt{3}}{2}\xi_s$, where $\xi_s$ is the sampling interval; therefore, two contour sections are considered to be approximately matched if equation (3.4) is satisfied. Subsequently, all points in $\{Sp\}$ are transformed, and the number of points that satisfy equation (3.5) are calculated. The best matching position is indicated by the largest number.

$$\xi(p, p') = \sum_{j=i-n}^{2n+1} (\sum_{k=1}^{K} \|p_j - p'_k\|^2) \tag{3.3}$$

$$\xi(p_i, p'_i) <= \frac{1}{2}\xi_s \cdot \sum_{k=1}^{K} \sqrt{2 + (k - \frac{1 + (-1)^k}{2})^2} \tag{3.4}$$

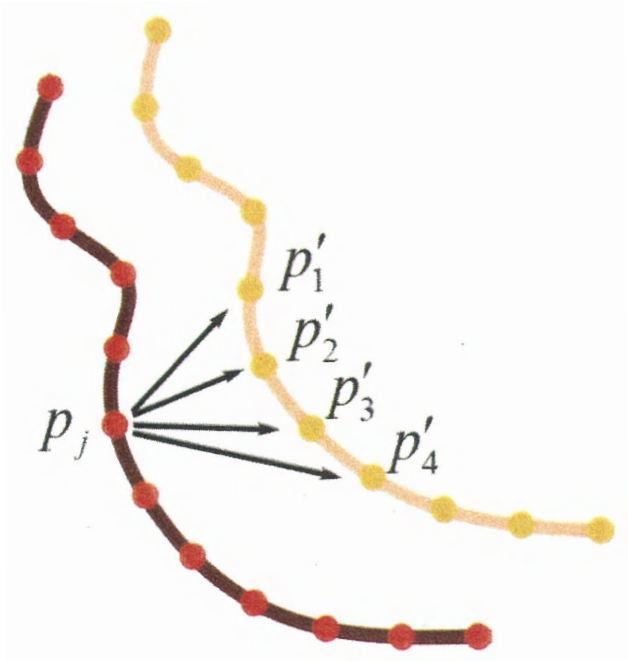


Figure 3.17: Matching two contour sections ($K = 4$).

$$\begin{cases} d(Sp_i, Sp') = min\{Sp_i - Sp'_j\} <= \frac{\sqrt{3}}{2}\xi_s, & (3.5) \\ d(Op_i, Op') = min\{Op_i - Op'_j\} <= \frac{\sqrt{3}}{2}\xi_s, & (3.6) \\ d(Op'_i, Op) = min\{Op'_i - Op_j\} <= \frac{\sqrt{3}}{2}\xi_s. & (3.7) \end{cases}$$

The next step is fine matching with the ICP algorithm. First, the original points set $O_p$ is transformed by $M_a$, and the number of near points is computed using equations (3.6) and (3.7) for both $S$ and $T$. The ICP algorithm is applied to the pair of near points to obtain the fine matching transform matrix $M_b$. Finally, the final matching transform matrix $M$ is calculated as $M_a \times M_b$.

### 3.4.4 Results

We implemented our proposed method using the C++ programming language on a PC with an Intel Core i7-4790 CPU and 8.00GB memory. Figure 3.18 compares the experimental results for pairwise partial matching of flakes obtained with the SHOT descriptor [2], S-ICP algorithm [1], and the proposed method. The two flakes examined in the experiment are shown in Figure 3.18(a), with the flake surfaces extracted and colored blue and red. Figures 3.18(b) and 3.18(c) show the SHOT and S-ICP results, respectively. The key-points correspondences with the SHOT descriptor are disordered, since the flake surface features are indistinct. The S-ICP algorithm also struggles to yield an accurate result, even though the initial position is adjusted manually. In contrast, our proposed method achieves a superb result, as shown in Figure 3.18(d). These experimental results demonstrate that our method is more suitable for flake models, which the existing methods struggle to resolve.

Three other flake pairs were also tested, and the results are shown in Figures 3.19, 3.20 and 3.21. In this figure, parts (a) and (b) show two original flake models, and part (c) shows the matched models. The detailed results are shown in Table 3.4. In these experiments, the scanning interval of the original point clouds was 0.1 $mm$, and the sampling interval $\xi_s$ was set to 1.0 $mm$. The parameters for computing the transform matrix were set to: $n = 8$ and $r = 2.0$. These matching results indicate that our method yielded excellent results for various flakes. The segmentation and downsampling employed in our method reduced the number of points necessary for the calculation efficiency. Furthermore, the short execution time proved that our method can efficiently process a large number of point clouds. Figure 3.22 shows an example of a matching assembly of seven stone tools, six stone tools are obtained superb results. The stone tool which cannot be matched is shown by the red arrows, since it has no adjacent surfaces with the others. The limitations of the proposed method are that the parameter $n$, the length of matching contour line,

is difficult to determine; it affects the efficiency and results of the algorithm. Besides, our method may not obtain correct results if the adjacent surface is cramped.

Table 3.4: Flake matching performance of the proposed method (Unit of length and time: mm, s).

| Flake | Length | Point number | Flake surface number |
|---|---|---|---|
| 1(a) / 1(b) | 72.0 / 100.3 | 263,112 / 382,861 | 4 / 3 |
| 2(a) / 2(b) | 63.0 / 69.4 | 406,674 / 345,481 | 3 / 3 |
| 3(a) / 3(b) | 64.5 / 80.6 | 272,038 / 319,595 | 2 / 4 |

| Pre-work time | Matching time | Total time |
|---|---|---|
| 6.3 / 10.6 | 96.5 | 113.4 |
| 12.1 / 9.7 | 51.4 | 73.2 |
| 15.0 / 11.5 | 44.8 | 71.3 |

## 3.5 Discussion

In this chapter, we proposed a new method for refitting mixture lithic materials by matching flake surfaces. Several characteristics were designed in our algorithm according to the principles of lithic material refitting. The experiment results could show that our new method could obtain precise refitting results for mixture lithic materials. To study more efficiency matching algorithms and the matching method for flakes that are matching each other on a extremely small part, we proposed an efficient method for pairwise matching flake models, in which the matching matrix is computed by constructing 4-points based on the contours and normals of the flake surfaces. In addition, we proposed an error function to measure the difference between two uniformly sampled contour lines. The experiments results indicated that our new method has beneficial applications for archaeological research.

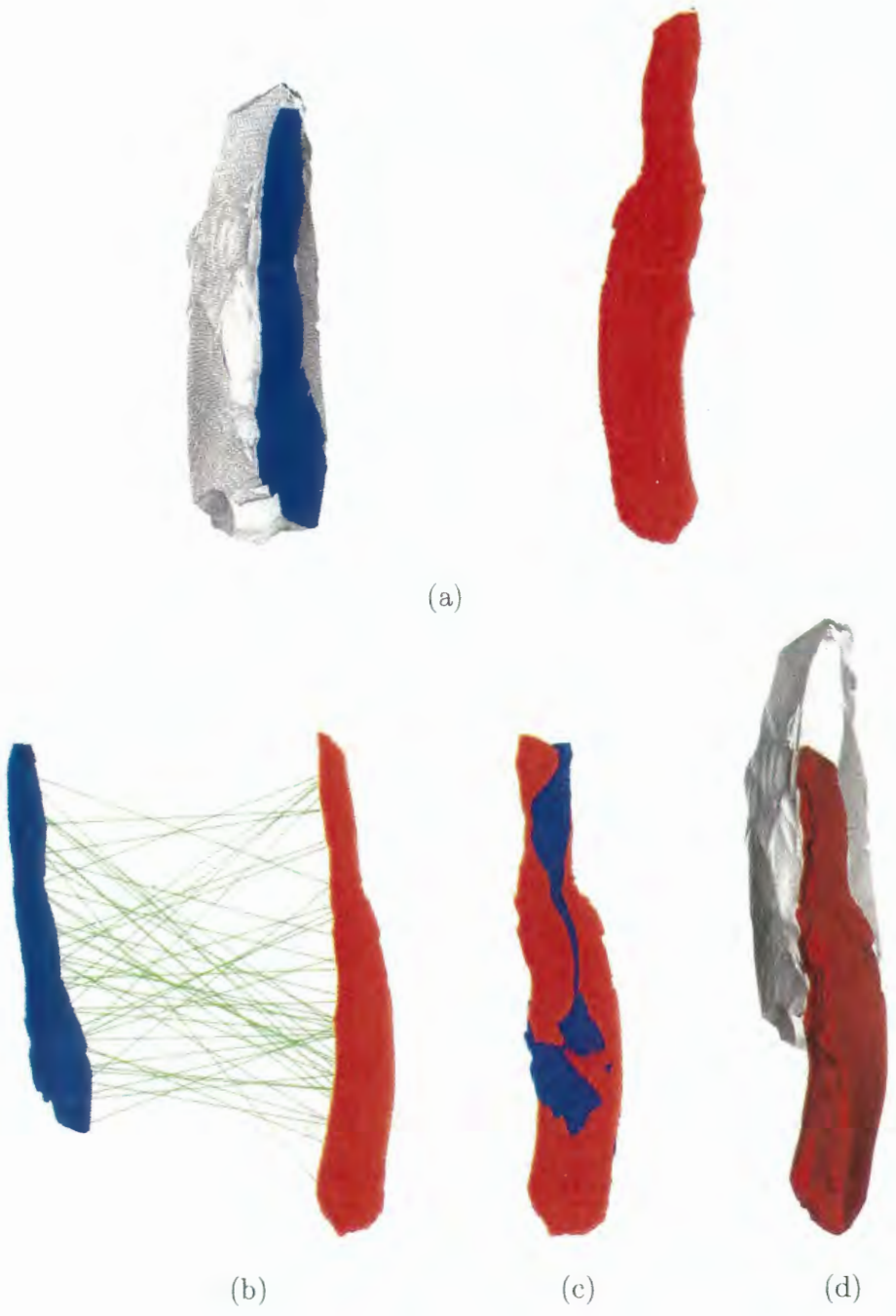


Figure 3.18: Comparison results. (a) Two original flakes ($Length = 72.0mm$, $80.8mm$). (b) Correspondences with SHOT descriptor (green lines). (c) The S-ICP registration result ($p = 0.4$, $iterations = 100$). (d) Matching result yielded by our proposed method.

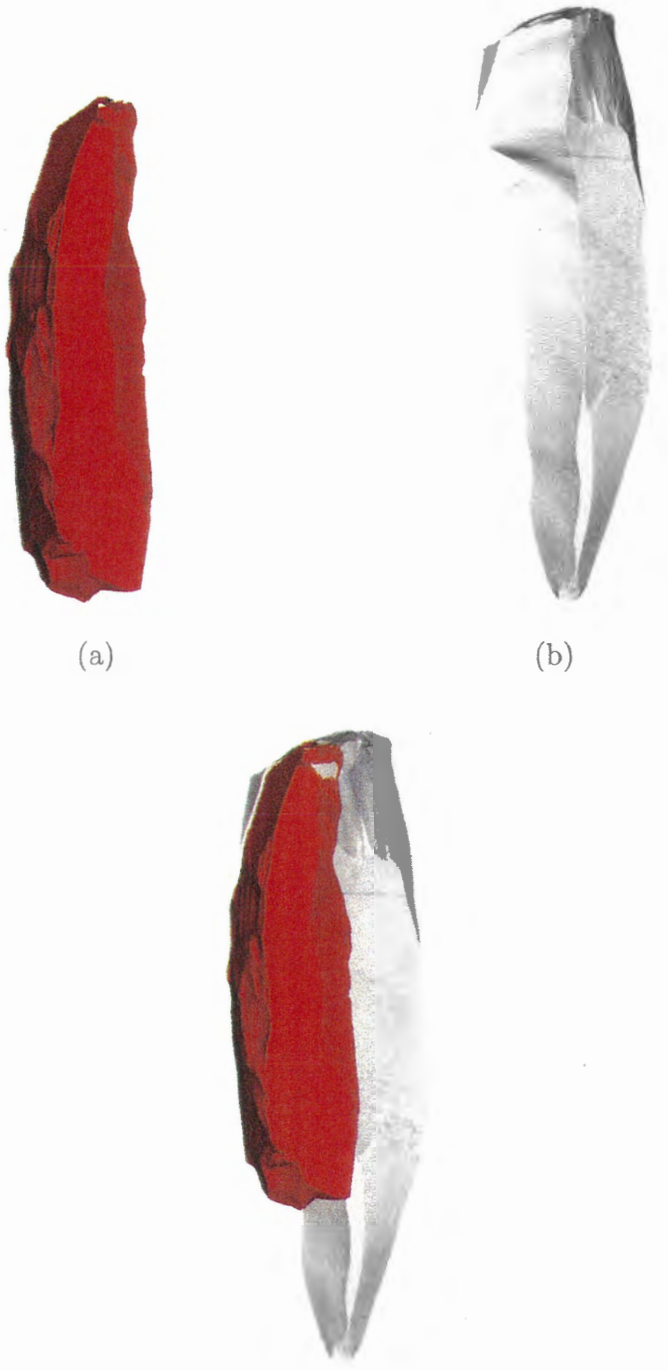

Figure 3.19: The first flake pair. (a) (b) Two original flakes. (c) Matched flakes.

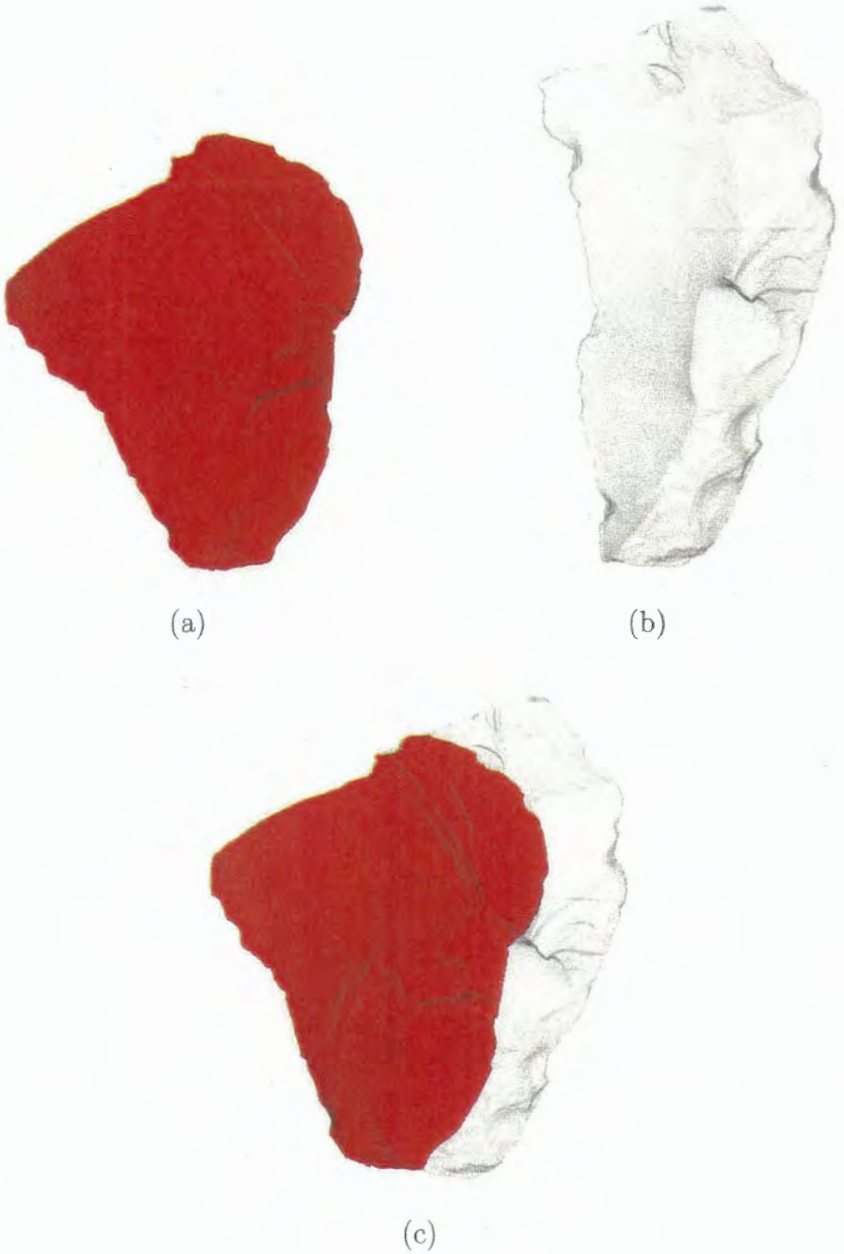

Figure 3.20: The second flake pair. (a) (b) Two original flakes. (c) Matched flakes.

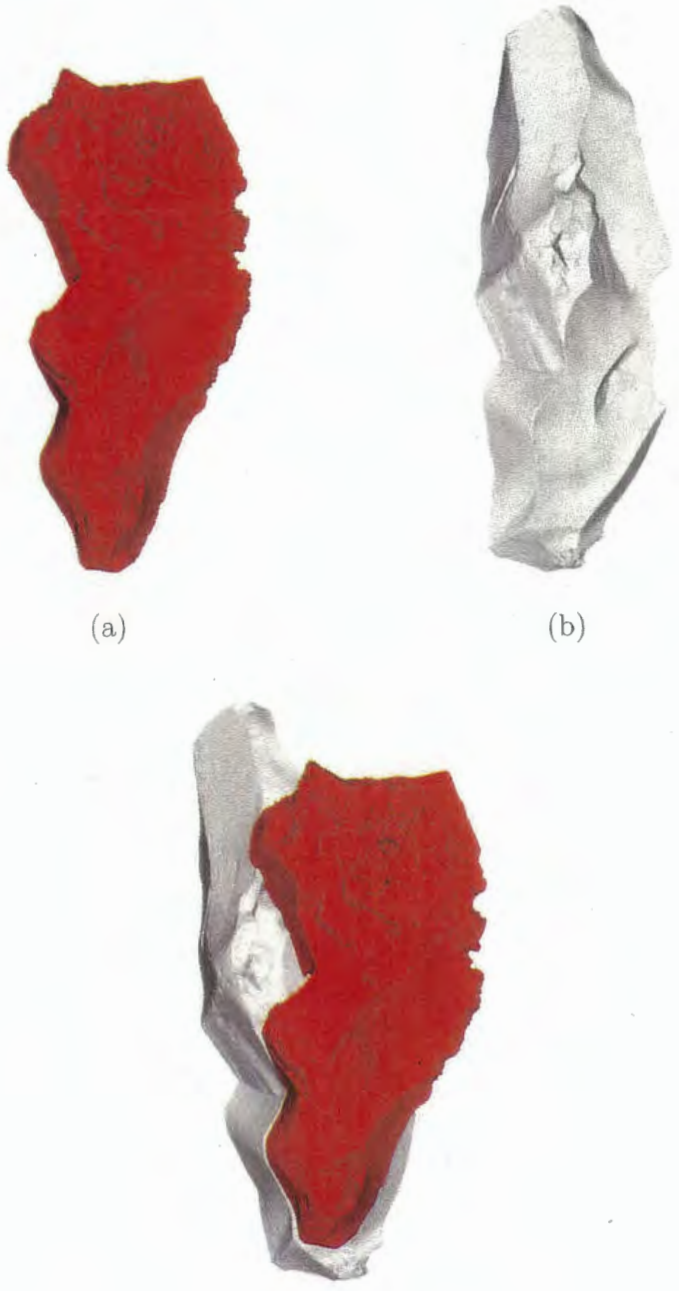

Figure 3.21: The third flake pair. (a) (b) Two original flakes. (c) Matched flakes.

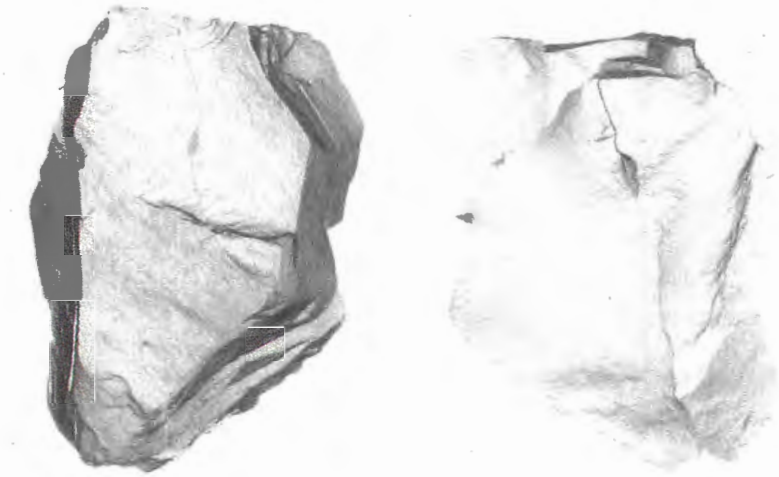

(a)

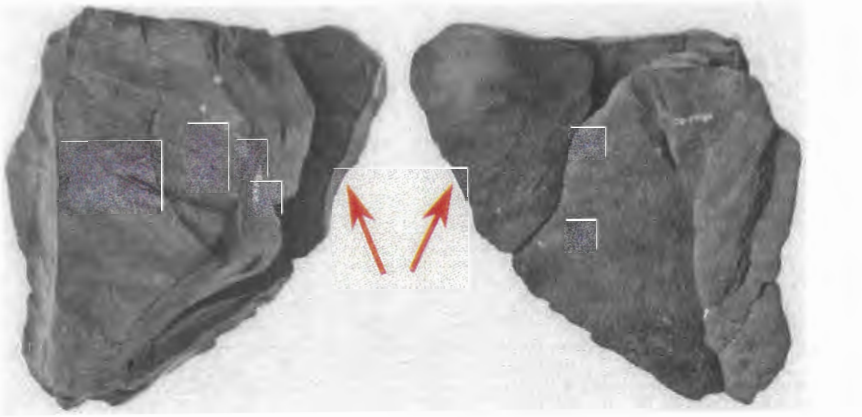

(b)

Figure 3.22: An example of a matching assembly of seven stone tools. (a) The screenshots of front and back view of matching result. (b) The pictures of actual assembly of stone tools.

# Chapter 4

# Visualization

## 4.1 Overview

This chapter introduces traditional illustrations for lithic materials in archaeology and 3D illustrative visualization technologies. According to archaeology rules, we study a visualization instruction for stone tool assembles based on point cloud to improve user experience. Our contributions include the following:

1. In addition to the design principles for automated generation of assembly instructions [7], we propose the principles for instructing the refitting of stone tools based on archaeological rules, whose details are described in Section 4.2.1.

2. In contrast with CAD models, the algorithms for point cloud are studied in order to automated generate exploded view and assembly sequence.

3. A comparative analysis is made between an automatically generated sequence and a flake knapping sequence in the archaeological report.

4. An interactive system is developed to assist archaeologists via step-by-step instruction and exploded view.

The three contributions are related as follows: item (1) is the elemental technology of our method and item (2) is for evaluation of the consistency between the result of item (1) and the content of the report. Furthermore,

when the result of item (2) is different from the user expectation, the intended information can be presented in the editing procedure using item (3).

## 4.2 Related Works

### 4.2.1 Lithic Technology and Traditional Illustration

When a stone tool is created, rock edges are struck repeatedly with a pebble, and flake pieces are obtained in various sizes as shown in Figure 4.1(a). Each of the flakes is peeled to adjust the stone tool shapes. A flake surface is an adjacent surface between two flakes, and the core is the remaining portion of the rock. Thus, assembly operation of a stone tool is restoration with the core and the flakes peeled from the same rock scattered over an excavation site. The flake knapping sequence represents the order in which flakes are peeled from the outside to the inside in stone tool creation [42]. In addition, when one flake surface may be divided into several pieces [103], part of the flake knapping sequence can be decided by considering reconstruction relationships. For example, as shown in the Figure 4.1(b), both Flakes $A$ and $B$ are adjacent to Core, but Flake $A$ should be peeled before flake $B$. This is because the flake surface $F_C$ is obtained by combining flake surfaces $F_1$ and $F_2$.

2D illustrations and photos are employed to depict the shapes and grain characteristics on lithic materials in the traditional archaeological literature [64]. Figure 4.2 shows traditional illustrations in an archaeological report [63]. A restored stone tool is exhibited in several 2D side views. Figure 4.2(a) depicts the details of the assembled stone tools, and in Figure 4.2(b), the pieces are labeled with identifying numbers. Archaeologists decide the flake knapping sequence by observing the real stone tools, and record it as $55 \rightarrow 58 \rightarrow 61a \rightarrow \cdots$. Although these pictures can be more accurately generated by a software [25], assisting hand-drawings, the shape of each stone tool and their position relationship are difficult to determine with such simple outlines. While the flake knapping information is explained more intuitive by 3D techniques, such as, 3D data display with flake ID, diagram viewers for assembly and separation direction and posture of flakes, a demonstration of flake knapping sequence.

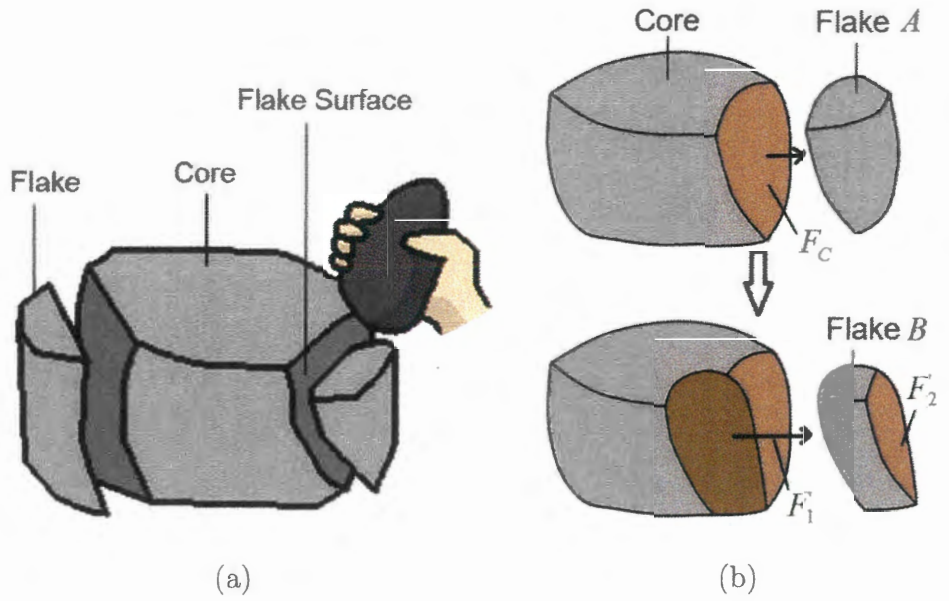


Figure 4.1: Making a stone tool.

### 4.2.2 3D Illustrative Visualization

The 3D exploded view diagram is a view that can separate an assembly using a specified order, orientation, and distance. The view can expose and analyze the inner structure of the assembly, and exhibit the position relationship between each part. Action diagrams can be generated to clearly depict the parts and the operation required in each assembly step using the exploded view [8]. Tatzgern et al. [92] and Li et al. [50] presented systems that automatically generate explosion diagrams of complex 3D CAD models. Lau et al. [47] developed a framework for generating parts that can be fabricated and connectors from 3D furniture models. Igarashi el al. [43] introduced an interactive system to assist the design and construction of 3D beadwork with a step-by-step guide. Karpenko et al. [45] presented a technique for visualizing complicated mathematical surfaces. Bruckner and Gröller [21] applied exploded views to volumetric data, then Balabanian et al. [14] introduced an interactive illustrative visualization for medical volume data. Furthermore, 3D illustrative visualizations have been developed for more functionality. Mitra et al. [60] illustrated the motions of individual parts and the interactions between parts, and an automated approach was presented to illustrate how mechanical assemblies work. Assembly and disassembly illustration is applied

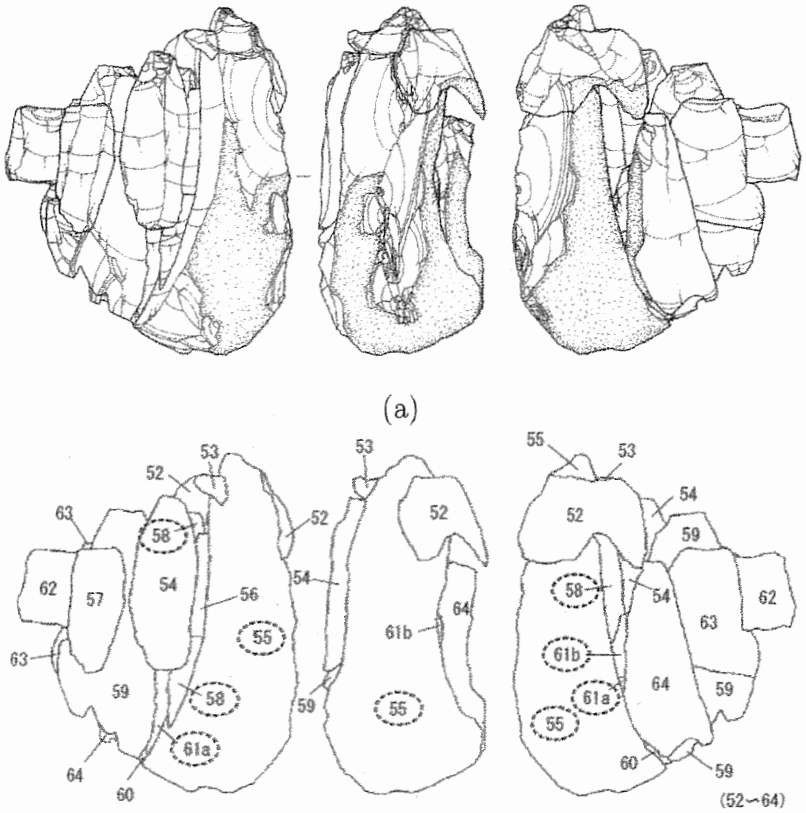


Figure 4.2: Traditional illustration of stone tools in a relic excavation report [63]. (a) The outline of the shape and grain characteristics of stone tools. (b) The identification of each stone tool by numbers.

to the design of a burr puzzle from a given 3D geometric model [98]. A computational solution is presented to support the making of interlocking furniture assemblies [29]. All of these methods using 3D visualization technology obtained superb instruction results as compared with manual work. However, it is simple to obtain the relationship and the exploded direction between adjacent parts for CAD designed models by input. While we have to study a method to calculate these basic informations for the point cloud models of stone stool.

## 4.3 Visualization Instruction

### 4.3.1 Our System

Our system is designed to comply with archaeological rules. To make a stone tool, the edge of a rock is struck repeatedly with a pebble, and flake pieces in various sizes are obtained as shown in Figure 4.1. The flakes are peeled to adjust the shape of the stone tool. The flake surface is the adjacent surface between two flakes, and the core is the remaining portion of the rock. Thus, an assembly of the stone tool is a restoration with a core and flakes peeled from a same rock that had been scattered all over an excavation site. The flakes are peeled in the order of outside to inside while creating a stone tool. Consequently, the assembly sequence should begin from the core and proceed to the outside in the reverse order. The input of our method is a set of matched point clouds $C$ created by scanning stone tools with roughly the same density, as shown in Figure 4.3(a). In addition, we assume that users already know which part is the core.

### 4.3.2 Constructing Explosion Graph

**Relationships.** The adjacent relationships of the parts being assembled are scored by the number of adjacent points with the Hausdorff distance smaller than $d_\varepsilon$. For each pair $C_i$ and $C_j$ of stone tools from $C$, it is assumed that the number of points in $C_i$ is smaller than $C_j$. $C_i$ and $C_j$ are regarded as adjacent models according to the number of adjacent points $A_{ij}$, which is more than $\alpha(\alpha < 1)$ times the number of points in $C_i$. The adjacent point $p_i$ from $C_i$ is computed by equation(4.1). To improve the robustness of the error metric, the mean distance of $k$ nearest points $p_j$ from $C_j$ is calculated for point $p_i$ from $C_i$.

$$d(p_i, C_j) = \frac{1}{k} \sum_{j=1}^{k} \|p_i, p_j\|^2 \tag{4.1}$$

By calculating and connecting the center points of each stone piece using the axis-aligned bounding box (AABB), the 3D adjacent relationship graph is obtained as shown in Figure 4.3(b).

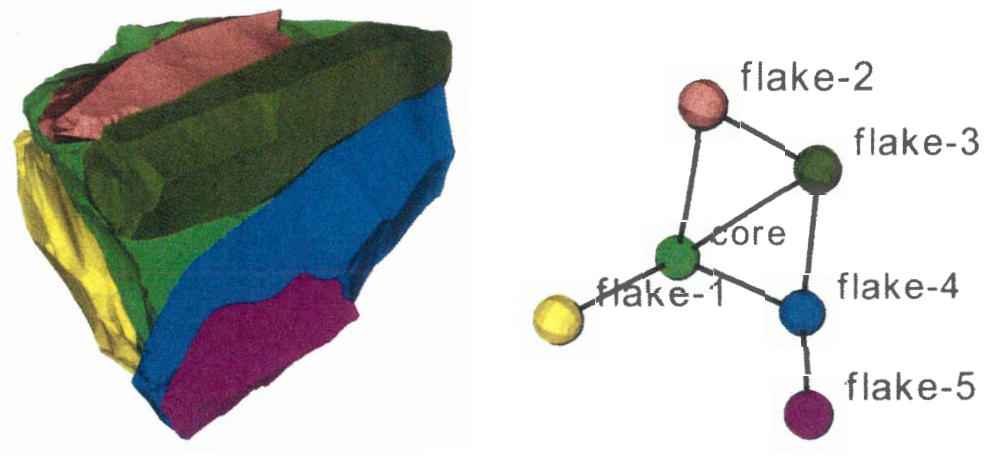


(a) (b)

Figure 4.3: Original input models and the generated adjacent relationships. Each sphere in (b) corresponds to the stone tool with the same color in (a).

Starting from the core of the assembly specified by a user, the undirected relationship graph can be converted to a directed graph as shown in the Figure 4.4(a). Then, according to the shortest path of each part, a hierarchical tree of the exploded graph is constructed in the Figure 4.4(b).

**Directions.** The flake surfaces of stone tools approach to a plane. Consequently, the exploded direction of each part is determined as an approximated normal vector of the adjacent points using the principal component analysis (PCA) on the center point. For example, in Figure 4.5, the red points represent the adjacent points $A_{ij}$, and the coordinate system is computed using equation(4.2). In this equation, $p_i$ is each point from $A_{ij}$ and $\bar{p}$ is the average point of all the adjacent points. The eigenvectors $v_1$, $v_2$ and $v_3$ of the covariance matrix $M_c$ represent the coordinate axes $z$, $y$ and $x$, respectively, corresponding to the eigenvalues of $\lambda_1$, $\lambda_2$ and $\lambda_3$ ($\lambda_1 \leq \lambda_2 \leq \lambda_3$). The exploded distance of each part is set by the user.

$$\begin{aligned} M_c &= \frac{1}{k}\sum_{i=1}^{k}(p_i - \bar{p})(p_i - \bar{p})^{\mathrm{T}}, \\ M_c \cdot v_j &= \lambda_j \cdot v_j, \\ p_i &\in A_{ij}, j \in \{1,2,3\} \end{aligned} \tag{4.2}$$

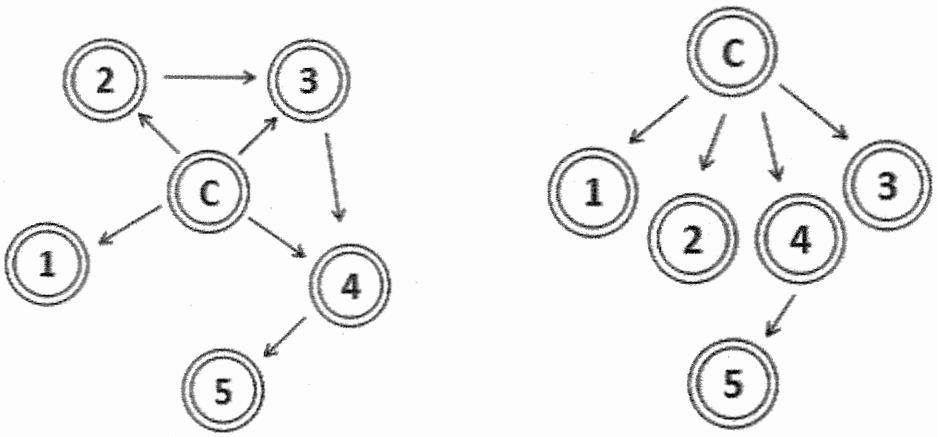


(a) (b)

Figure 4.4: The directed relationship graph and generated hierarchical tree.

### 4.3.3 Generating Assembly Sequence and Interactive Control

The exploded order is determined by the breadth-first-search (BFS) algorithm of the hierarchical tree from root; however, it is difficult to determine the order of the parts that belong to the same node. For example, the order of *flake*-6 and *flake*-7 that shown in the Figure 4.6. Under the circumstances, our system has a certain degree of freedom in which archaeologists can interactively control the generated assembly order. The stone tool of *flake*-6 is picked by mouse and is marked in red as shown in the Figure 4.7(a). Its position can be exchanged by keyboard without affecting the adjacent relationships between flakes shown in the Figure 4.7(b). Then, the assembly sequence of stone tools is exhibited via a visualized step-by-step instruction.

### 4.3.4 Flake Knapping Sequence Analysis

Starting from the core of the assembly specified by a user, the undirected relationship graph can be converted to a directed graph. In the previous work [104], a hierarchical tree is constructed as shown in the Figure 4.8(b), according to the shortest path of each part of the directed graph. The exploded order can be determined by the breadth-first-search (BFS) algorithm of the

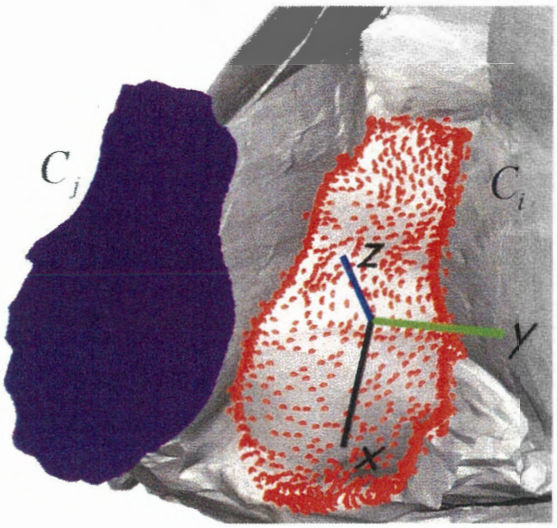


Figure 4.5: Calculation the coordinate system of a flake surface from adjacent points.

hierarchical tree from root. Then, the assembly sequence of stone tools is exhibited through a visualized step-by-step instruction.

In the previous work, the problem of the order of the parts that belong to the same node is solved by an interactive control. By introducing the detection of flake surface reconstruction described in the Section 3.3.4, this problem can be solved very well in most cases. For example, let us consider the order of $flake-6$ and $flake-7$ that shown in the Figure 4.8. Obviously, $flake-7$ should be peeled before $flake-6$ because $flake-2$, $flake-3$ and $flake-6$ are reconstructed to match with $flake-7$. In order to display the relationship of flake surface reconstruction, a relationship graph is employed instead of the hierarchical tree as shown in Figure 4.9, and node $R$ is inserted before each reconstruction flake for highlighting such relationships.

In addition, the flake knapping order of some stone tools is difficult to determine since the stone tools are not adjacent to each other. Figure 4.10 shows an example in the relic excavation report [63], where a part of the recorded sequence is $\langle 485\rangle\langle 487\rangle\rightarrow 489\rightarrow 488\rightarrow 486\rightarrow 490\rightarrow\langle 492\rangle\langle 491\rangle\cdots$, and symbol $\langle\bigcirc\rangle$ is employed to express unknown context. In other words, we cannot decide the order of peeling. Consequently, our system provide a function that enables free editing of flake knapping sequence.

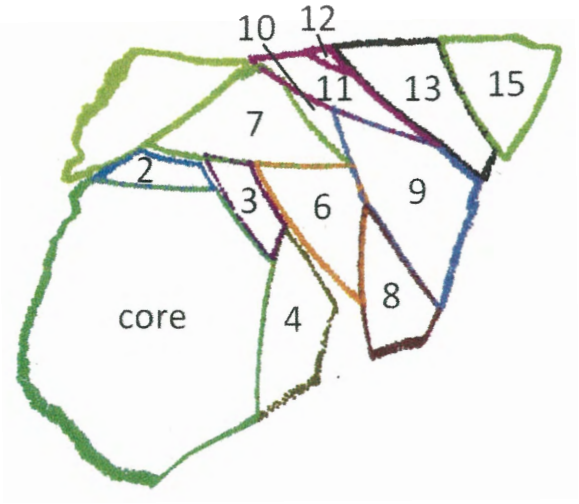


Figure 4.6: A cross section of the assembly of stone tools.

### 4.3.5 Exporting Animation

According to archaeological conventions, the animation of the rotating separation of a flake is also generated as shown in Figure 4.11 for recreating the making of a stone tool. The yellow arrow of Figure 4.11(a) displays the striking point. Figure 4.12 explains the computation of the transform matrix for a flake surface. The striking direction is approximated along the $x$ axis, and $l$ is the maximum distance between the center point and the edge of the flake surface. The rotation center $P_r$ is selected $\varepsilon \cdot l$ ($\varepsilon > 1$) away from the center point. The rotation axis is along the $y$ axis. Thus, the transform matrix $M$ is computed by a translation and a rotation, as described by equation(4.3). If the calculated striking direction has an error, it can also be set interactively.

$$M = T \times R \tag{4.3}$$

## 4.4 Results and Evaluation

### 4.4.1 Results

We have implemented the proposed method on a PC with Intel Core i7-4790 CPU and 8.00GB memory, the C++ programming language is used with Visual Studio 2013 and Windows 7. The assembly of group 1 consists of 18

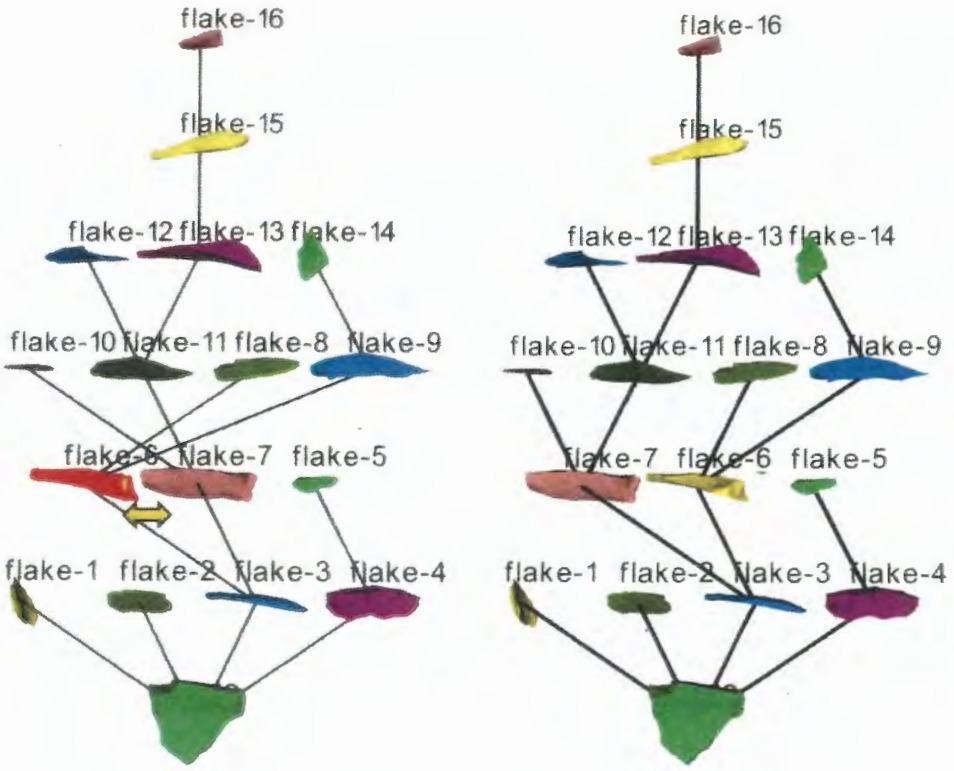


(a) (b)

Figure 4.7: Interactively generating the assembly order of stone tools. The *flake*-6 is selected and marked as red as shown in the left figure. The position of *flake*-6 is exchanged with *flake*-7 as shown in the right figure(*flake*-6⇔*flake*-7).

stone tools and the assembly of group 2 consists of 12 stone tools. The original models are shown in Figure 4.13. For groups 1 and 2, the average number of points in an object is about four thousands and ten thousands. The threshold $d_\varepsilon$ and $\alpha$ for the relationship calculation are set as $\{1.0, 0.02\}$ and $\{0.5, 0.01\}$, respectively. The computation time lengths are about 12.3 seconds and 3.1 seconds. Figures 4.14 and 4.15 display the 3D exploded diagrams for the two assemblies. The space positions of the models and adjacent relationships between the restored stone tools are powerfully visualized in the 3D exploded diagrams.

Figures 4.16 displays the relationship graphs with reconstruction relationships for groups 1 and 2. Four reconstruction relationships are detected in

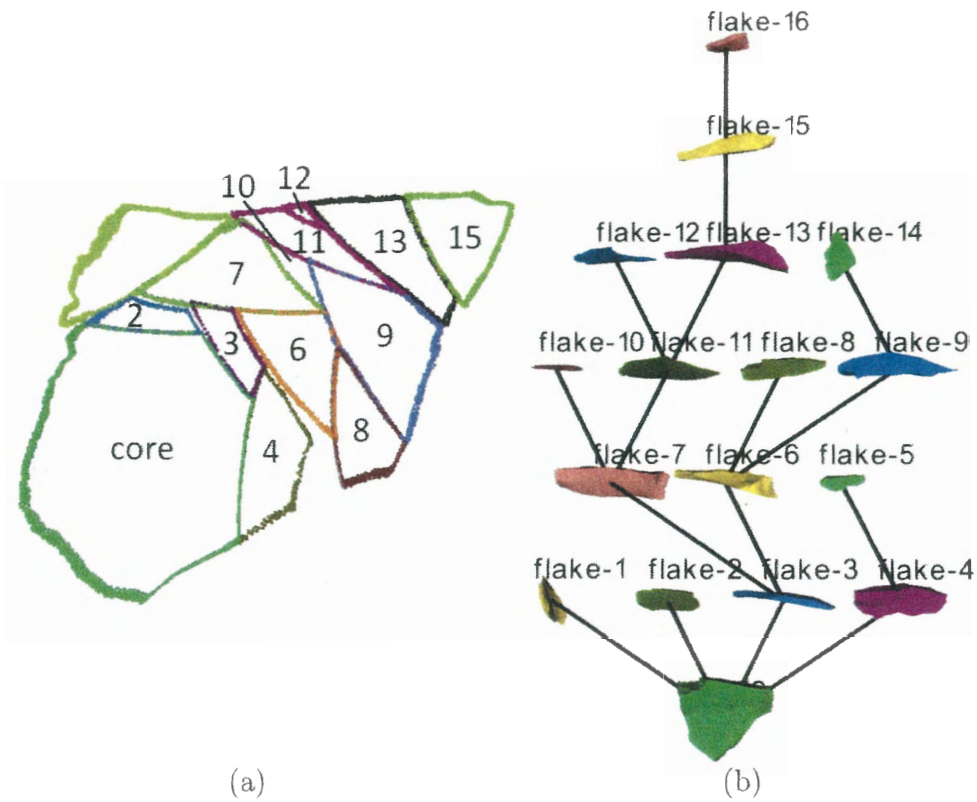


(a) (b)

Figure 4.8: (a) A cross section of the assembly of stone tools. (b) A constructed hierarchical tree from the relationship graph of the assembly of stone tools.

group 1 and six in the group 2. According to the information of reconstruction surfaces, ambiguous flake knapping sequence can be decided in most cases.

Figure 4.17 presents each step of the assembly process for group 2. Figure 4.18 presents each step of the flake knapping process for group 2. Our system could automatically generate the flake knapping sequence, and the sequence can be edited by user. The experiment results demonstrate that our system automated generation of exploded views for the assembly of stone tools, and the assembly or separation operation is exhibited distinctly via the step-by-step instruction.

In addition to conventional materials of archaeology, trace patterning can be more objective with utilizing 3D data obtained by measurement. It can make a contribution to stone certification theory, model theory and the analysis of manufacturing traces. Besides, it is necessary to mutually verify con-

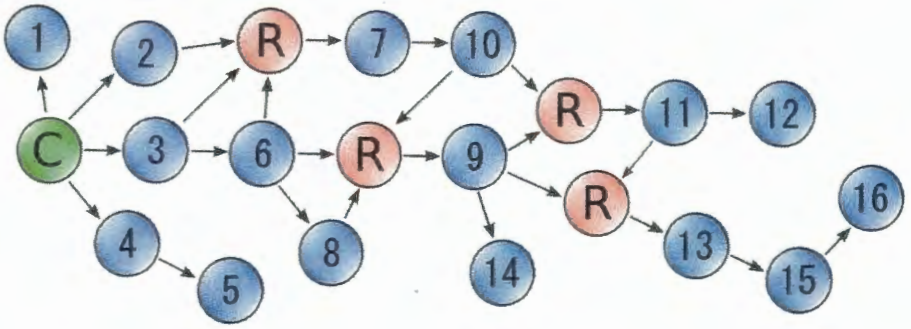


Figure 4.9: A relationship graph including the reconstruction relationships.

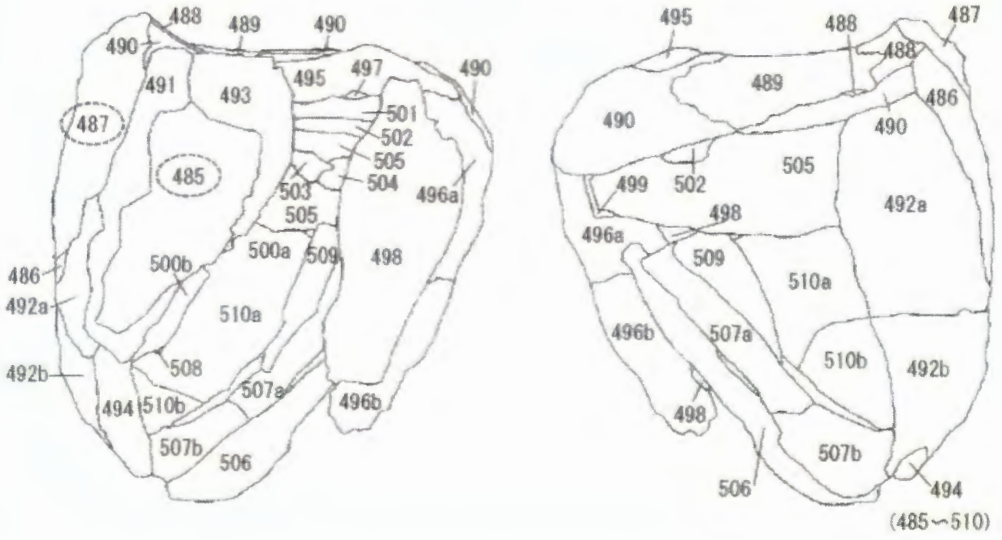


Figure 4.10: An example from the relic excavation report [63].

struction of assembling algorithms and deciphering of stone fabrication technologies. Our system assists archaeologists to reproduce the making process of stone tools repeatedly and observes the peeling traces between adjacent flakes.

### 4.4.2 Evaluation

For the user evaluation, all models of group 1 and 2 are fabricated by 3D printer. Two experiments are designed to evaluate our system. In the first experiment, we compared the reassembly time of stone tools with three methods: no reference, traditional illustrations, and our system. We invited six users as

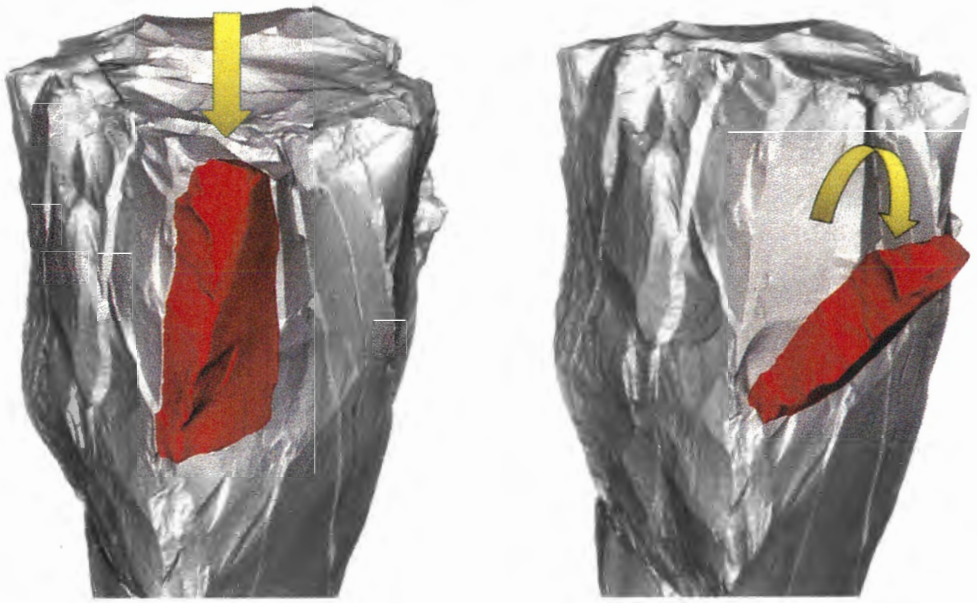

(a) (b)

Figure 4.11: Rotating separation of a flake, the striking point is shown as the yellow arrow in (a). Here, the yellow arrows are added to the screenshots of results in order to show the striking point and express the direction of separation clearly.

our subjects who have no experience with this research. The experiment time was limited to an hour. Each method was tested by two subjects, and each subject could not reassemble one group twice to avoid memory. Figure 4.19 shows the recorded average reassembly times, group 1 cannot reassembled without reference in an hour.

We invited four subjects to carry out the second experiment. Each subject compared the feeling of reassembly referring to traditional illustration with our system for one group. Two questions are designed in our questionnaire. Question 1 is, score the comprehension for understanding the guidance and applying it on the assembly. Question 2 is, score the helpfulness between the traditional illustration and our system. The result of the comparison is shown in Figure 4.20. For the feedback of subjects, they said it is easy to recognize which one should be reassembled in the next step, and 3D exploded diagrams clearly show the position and posture of assembly.

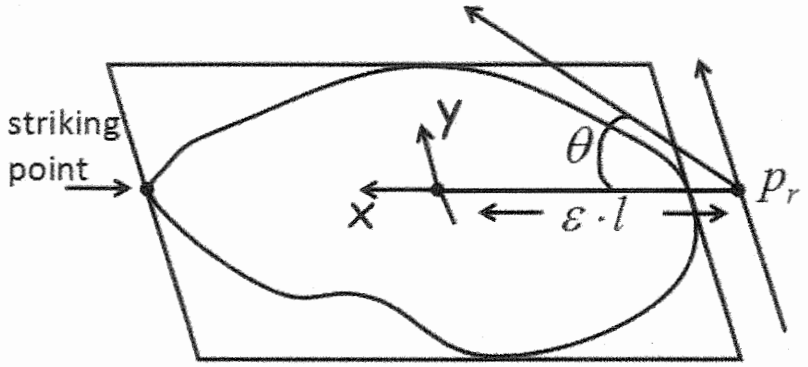


Figure 4.12: Calculating the transform matrix of separation.

We also invited two experts to evaluate our system. They think our system can greatly assisting in assembly and separation of stone tools. The automatic generated flake knapping sequences are consistent with the principles of archeology, and can be corrected easily.

## 4.5 Summary

In this chapter, we proposed a visualized instruction method of assembly sequence and flake knapping sequence for the assembly of stone tools. The visualization system is designed based on archaeological conventions, and it can favorably meet the needs of archaeological research. The user evaluation indicates that 3D visualization technology can assist in efficient research of flake knapping sequence instruction for chipped stone tools.

Figure 4.13: Original models of group 1 and group 2.

(a) (b)

Figure 4.14: 3D exploded diagram of group 1.

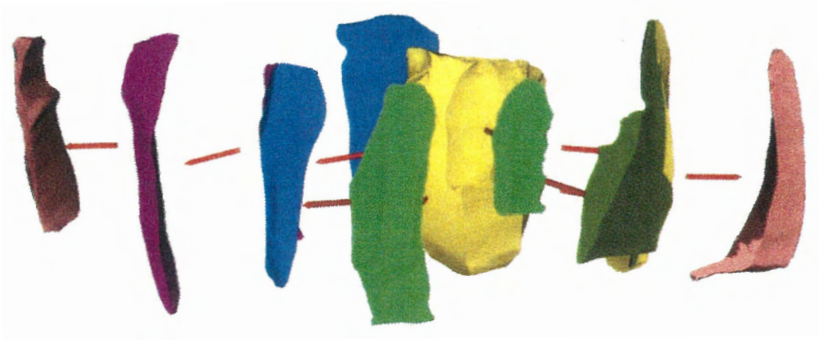

(a)

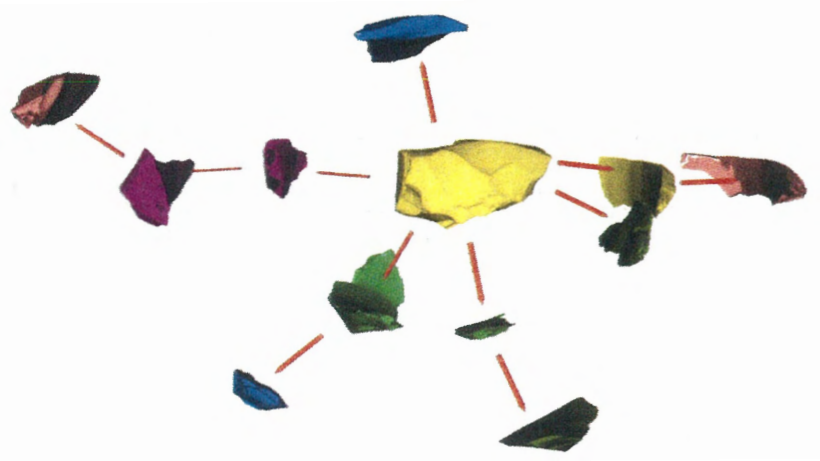

(b)

Figure 4.15: 3D exploded diagram of group 2.

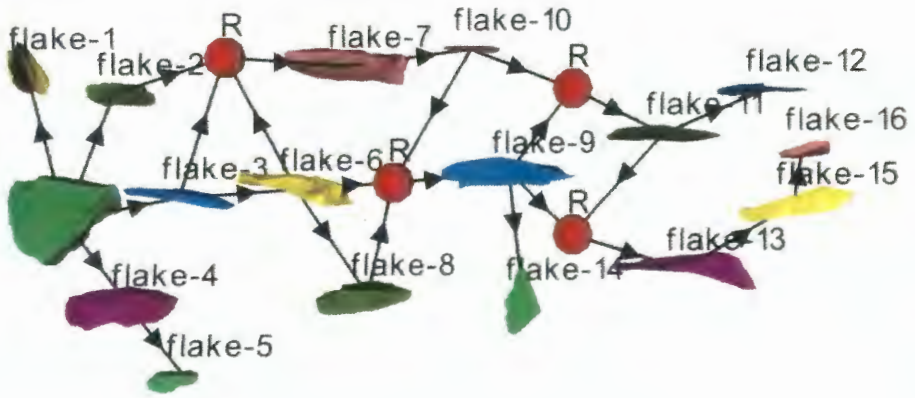


(a)

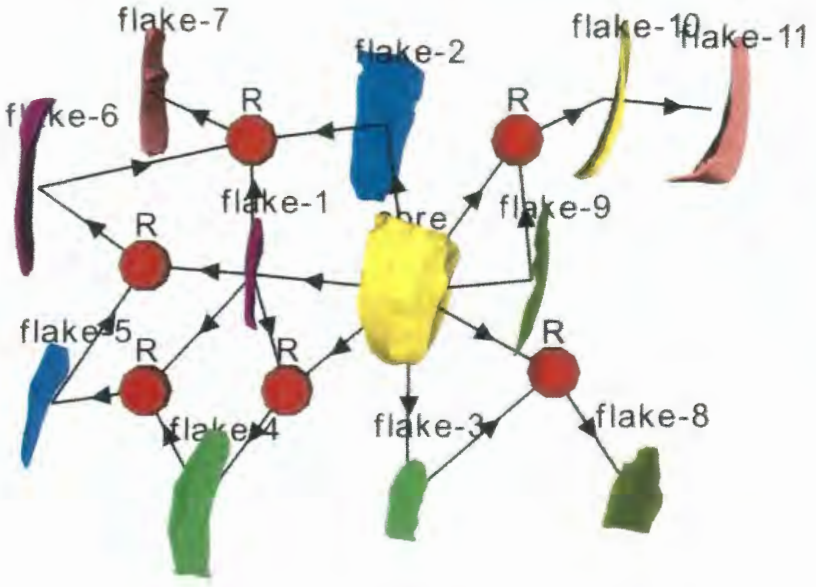


(b)

Figure 4.16: (a) 3D relationship graph for group 1. (b) 3D relationship graph for group 2. The red spheres show reconstruction relationships and the arrows indicate assembly directions.

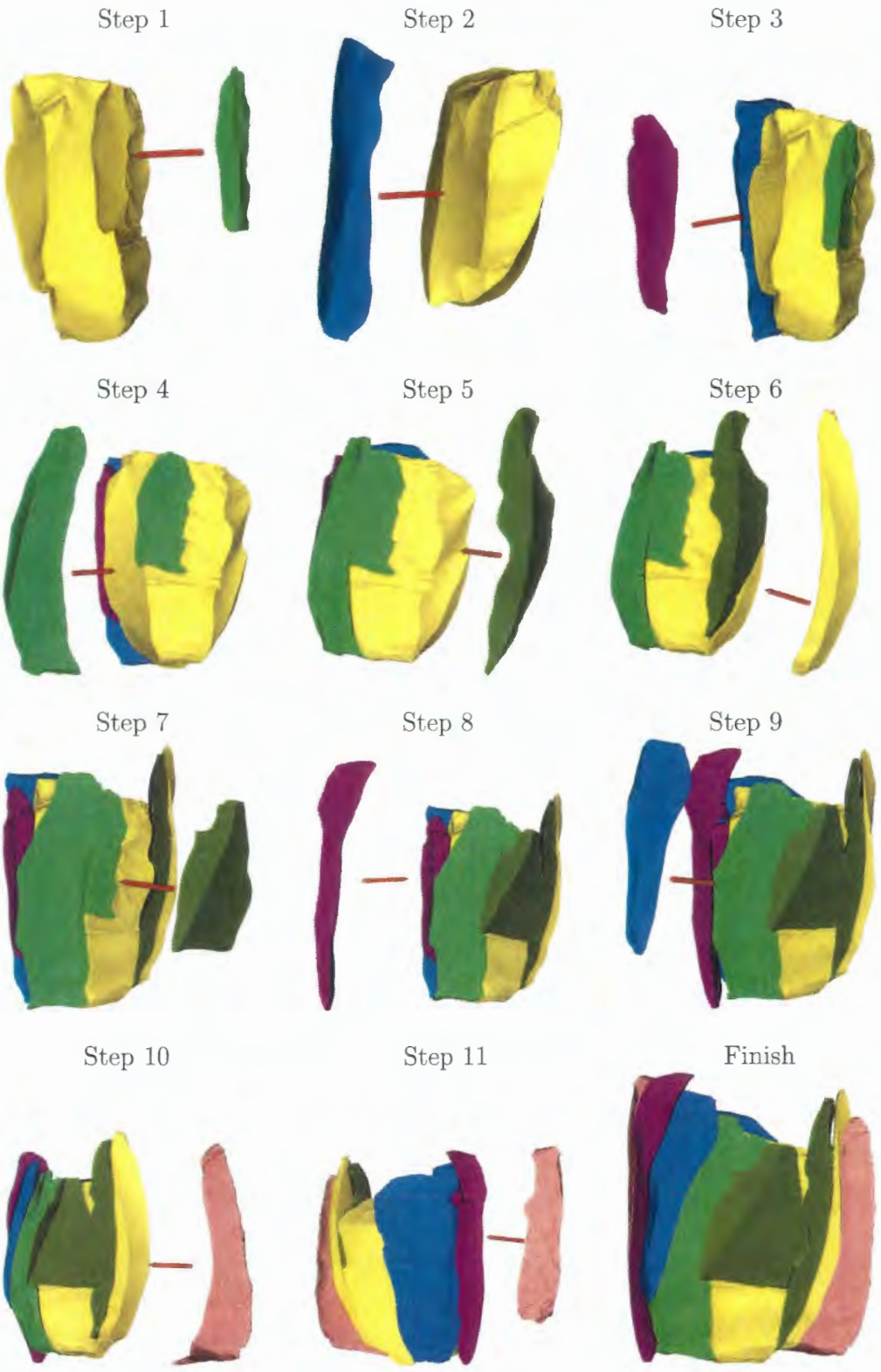


Figure 4.17: Assembly instruction with a step-by-step guide for group 2.

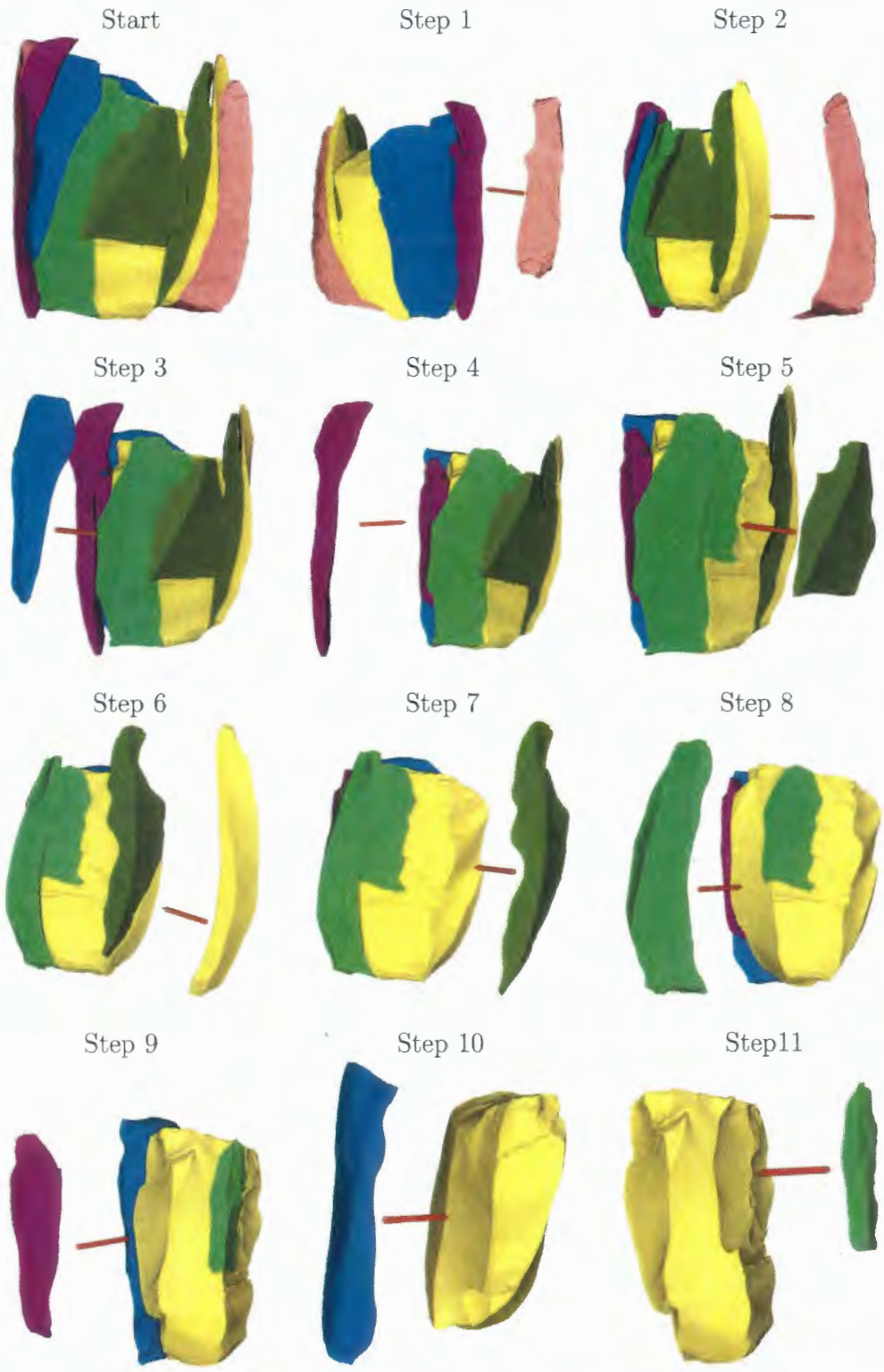


Figure 4.18: Flake knapping sequence instruction with a step-by-step guide for group 2.

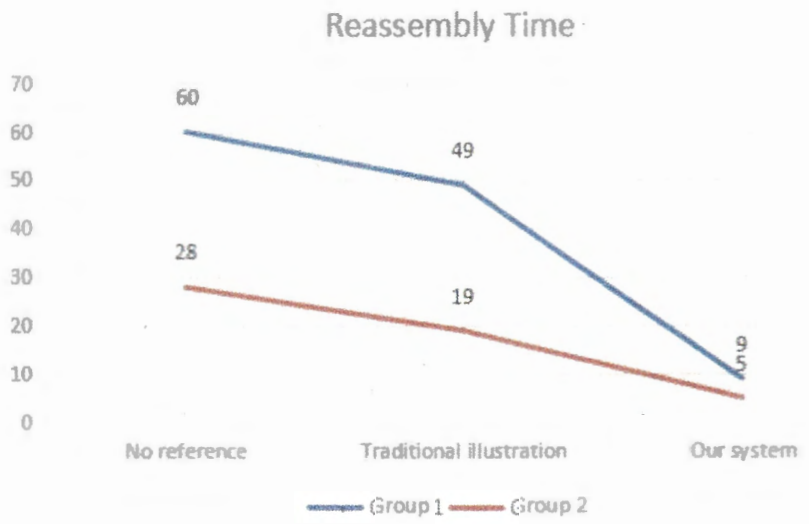


Figure 4.19: The reassembly times (min).

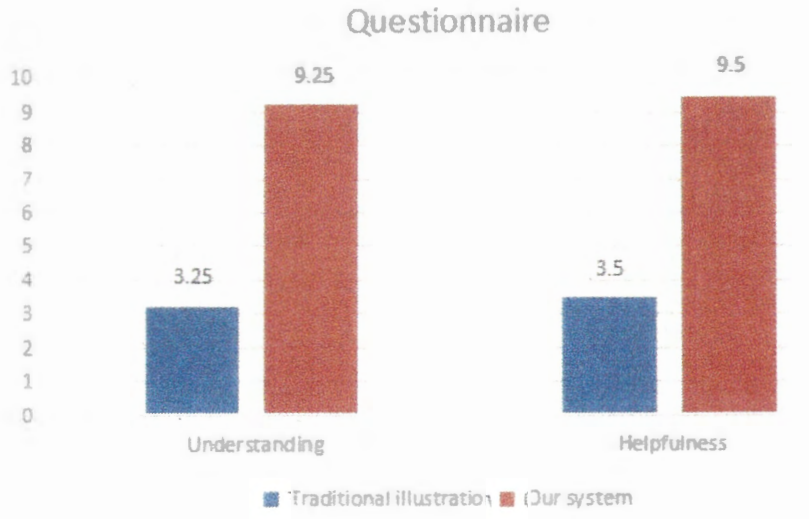


Figure 4.20: The result of questionnaire.

# Chapter 5

# System Architecture

We use C++ to implement our system, there are two popular development tools for point cloud processing: the Computational Geometry Algorithms Library (CGAL) [5] and the Point Cloud Library (PCL) [4] , PCL is chosen to build a framework in our research.

## 5.1 The Preparation Work Tool

A tool is built to assist in preparation work of refitting lithic materials, as shown in Figure 5.1. The result of each algorithm is obtained by choosing a function and inputting the parameters which are needed. The functions include:

- Segment all of the point cloud data in a folder into flake surfaces. A new folder named "segmented" is created in the folder of data, and the segmented flake surface files are put into each folder named by the original data file, as shown in Figure 5.2. Parameters: $ST$ (Smoothness Threshold), $CT$ (Curvature Threshold), $SR$ (Segmentation Rate).

- Segment one point cloud data into flake surfaces. Parameters: $ST$ (Smoothness Threshold), $CT$ (Curvature Threshold), $SR$ (Segmentation Rate).

- Simplify all of the flake surface data in a folder. A new folder named "simplified" is created in the folder of original data, and the simplified

flake surface files are put into each folder named by the original data file, as shown in Figure 5.2. Parameters: *DT* (Distance Threshold).

- Simplify one flake surface data. Parameters: *DT* (Distance Threshold).
- Extract the contour line of all of the flake surface data in a folder. A new folder named "contour" is created in the folder of original data, and the contour line files are put into each folder named by the original data file. Parameters: *DT* (Distance Threshold).
- Extract the contour line of one flake surface data. Parameters: *DT* (Distance Threshold).
- Make the normal vectors of a flake surface consistent. Parameters: *None*.
- Reverse the normal vectors of a flake surface. Parameters: *None*.
- Display a point cloud data with normal vectors. Parameters: *None*
- Display a contour line with numbers. Parameters: *None*
- Create data for Bayer's pairwise matching method. Normal vector ($vn$) and curvature ($m$) are calculated for each point, and flake surfaces ($c$) are segmented. Parameters: *ST* (Smoothness Threshold), *CT* (Curvature Threshold), *SR* (Segmentation Rate).
- Calculate feature points of a point cloud by Bayer's curvature computing method. Parameters: *CT* (Curvature Threshold).

In addition, some functions have not been integrated into this tool.

- Re-sampling a point cloud by Moving Least Squares (MLS) . Parameters: *Radius*.
- Down-sampling a point cloud by Voxel Grid. Parameters: *LS* (Leaf Size).
- Smoothing a contour line. Parameters: *None*
- Making normal vectors of a point cloud outward. Parameters: *None*
- Determining a flake surface if concave. Parameters: *None*
- Decompose and merge polygon mesh data. Parameters: *None*

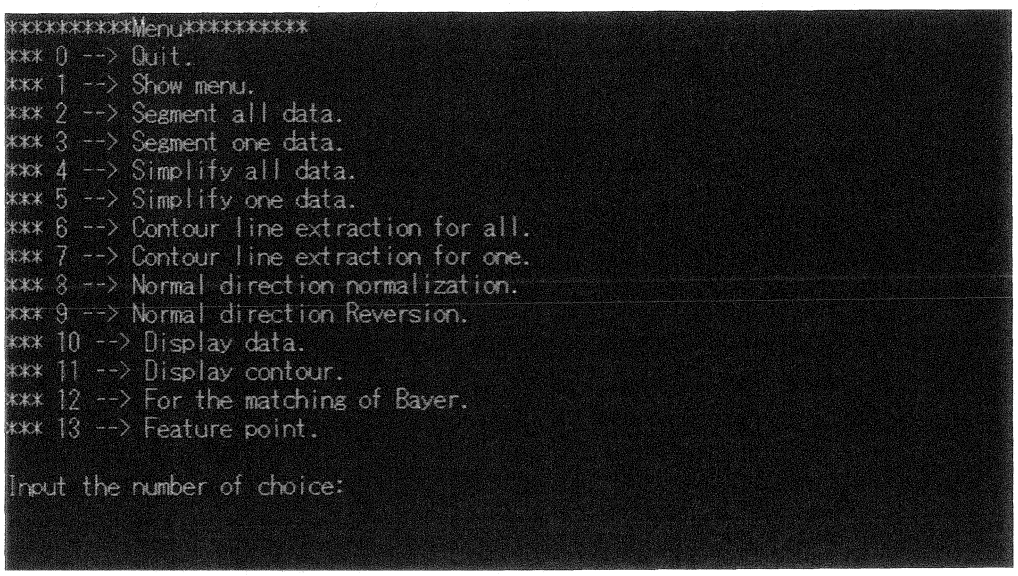


Figure 5.1: The preparation work tool.

## 5.2 Matching System

The matching system is designed to consist of two viewers: waiting viewer and matching viewer, as shown in Figure 5.3. At first, all of the flakes are shown in the waiting viewer sorted by calculating the concave and convex ratio of flake surfaces, because a flake which flake surface are all concave is regarded as a core. Six flakes are shown in once time, their names are marked in the lower left corner, as shown in Figure 5.4. Then the user can select a core as a start point, and it will be shown in the matching viewer, as shown in Figure 5.5. Next, the user selects a flake surface to start the matching algorithm to search the matching flake surface. The waiting viewer will show the candidates sorted by matching degree.

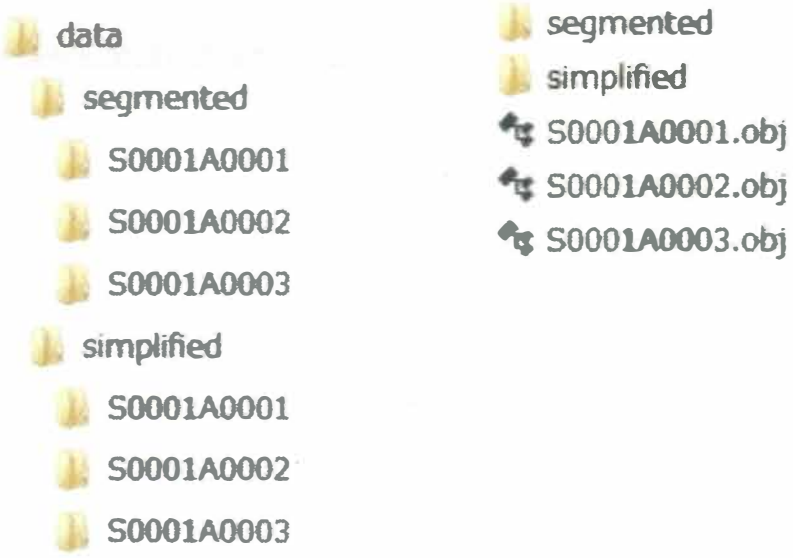


Figure 5.2: The folder structure.

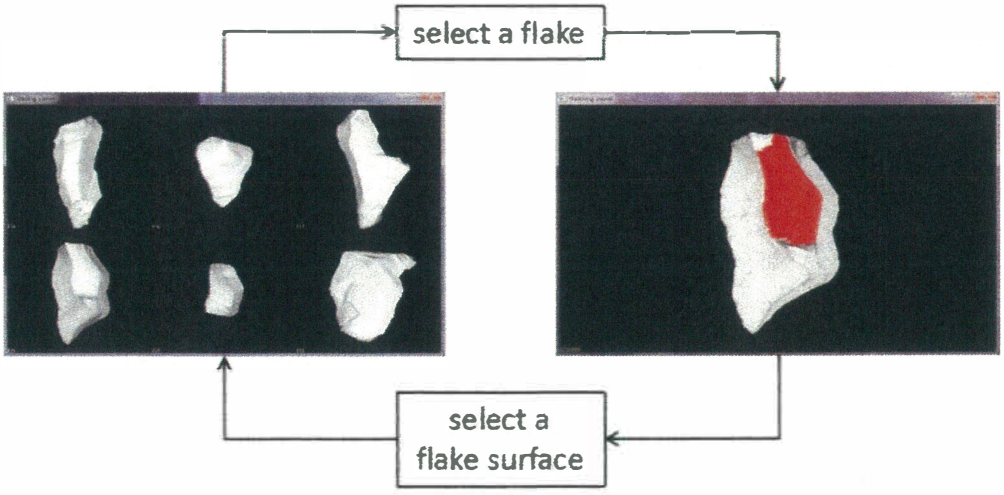


Figure 5.3: The workflow of system.

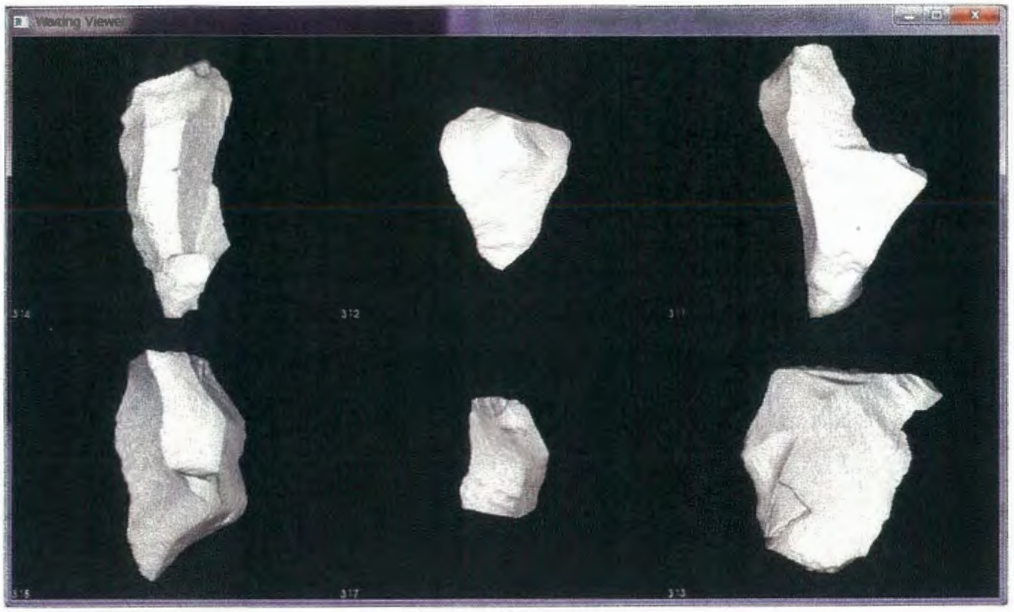


Figure 5.4: Waiting viewer.

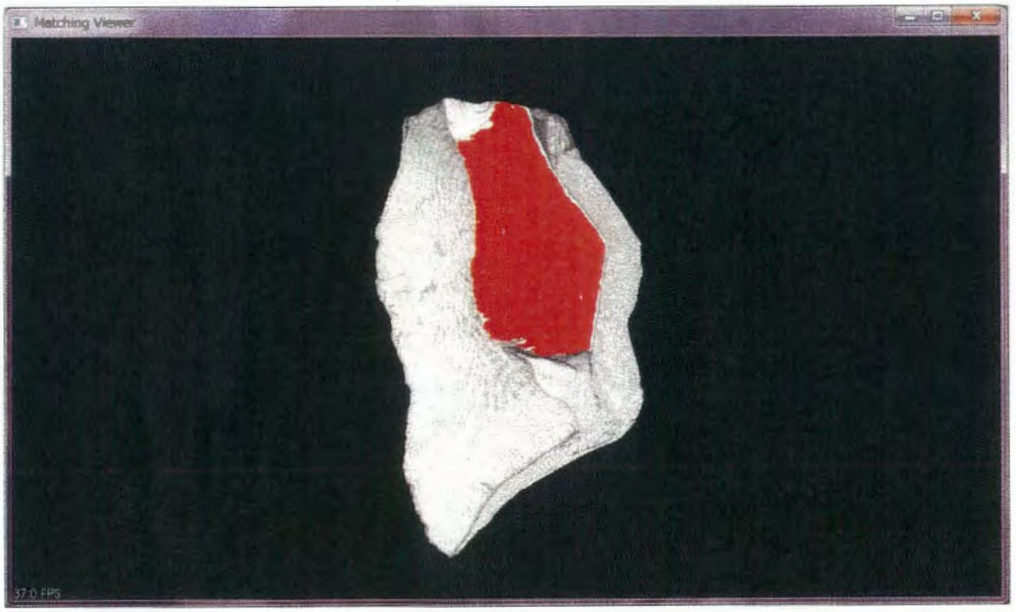


Figure 5.5: Matching viewer.

# Chapter 6

# Conclusions and Future Work

## 6.1 Conclusions

Computer graphics has a wide application prospect in archaeology and cultural heritage. In this thesis, we focus on studying measured 3D point cloud techniques for refitting lithic materials in two aspects: matching and visualization. In chapter 1, the background and importance of refitting lithic materials research are explained. In chapter 2, the related point cloud processing algorithms are summarized at first as the foundation of our research. Then, the state-of-the-art related works are introduced in digital technologies apply to archaeology and cultural heritage.

In chapter 3, a method is proposed to refitting lithic materials by matching flake surfaces based on triangle mesh. Firstly, the flake surfaces are segmented from each flake. Next, each flake surface is simplified to reduce computation. From a core, the best matching is searched for a flake surface by pairwise matching. The divided flake surfaces are also detected to reconstructed into one. As the same pipeline, the point cloud method is studied by some adjustments to improve efficiency. The judgment condition of best matching position is changed to handle partial matching.

Matching by segmented flake surfaces is an intuitive idea, however, it has to do trivial pre-treatment works. Additionally, the data has some measurement problem that leads the system of matching flakes more difficult to realize automatic. Furthermore, the needed information beyond the flake surface

will be a bottleneck for further research. To avoid these problems, matching flakes by the whole object may be a solution, although it would be very hard at the beginning.

In chapter 4, the exploded view diagrams are used to visualize instruction for the assembly and separation of stone tools. The exploded graph, exploded direction, assembly sequence and flake knapping sequence are calculated based on point cloud. An interactive system is designed to edit the generated order, and then, the reconstruction relationship is employed to solve ambiguous order. This is just a start in a visualization of assemblies of stone tools.

We use C++ to implement our proposed methods and tested with lithic material 3D models. PCL library is chosen to build a framework. Two groups of stone tools are efficiently finished through our matching method by refitting materials from the mixture of several groups. The limitation of this method has been solved by the next research. These experimental examples indicated that the matching methods can achieve superior matching results. After that, the explosion graphs of two groups are generated, and the assembly and separation sequences are computed and analyzed. The experimental results of stone tool assemblies indicate that 3D visualization technology can assist in the efficient research of assembly and separation instruction of stone tools for chipped stone tools. A tool is developed to deal with the preparation works, and a visualization matching system is built as described in chapter 5.

## 6.2 Future Work

For the matching study, our proposed method will be applied as an archaeological assistant system to identify and match fragments of massive stone tools. Through a large number of tests on excavated relics, not only is our method improved but also new archaeological discoveries are made since the matching result of stone tools greatly affects the analysis of manufacturing technique and relationship between each site.

For the visualization instruction, we will further study the effectiveness of the proposed method by applying it to massive data, and we will expand our system so that it can be widely applied to the assembly visualizations in archaeology.

# Bibliography


[1] Sparse iterative closest point. `http://lgg.epfl.ch/sparseicp`, 2013.

[2] SHOT descriptor in point cloud library (pcl). `http://pointclouds.org/documentation/tutorials/correspondence_grouping.php`, 2014.

[3] Fast triangulation of unordered point clouds. `http://pointclouds.org/documentation/tutorials/greedy_projection.php`, 2015.

[4] The Point Cloud Library (PCL). `http://pointclouds.org/`, 2015.

[5] The Computational Geometry Algorithms Library (CGAL). `https://www.cgal.org/`, 2018.

[6] T. Adamek and N. O'Connor. Efficient contour-based shape representation and matching. In *Proceedings of the 5th ACM SIGMM international workshop on Multimedia information retrieval*, pages 138–143. ACM, 2003.

[7] Maneesh Agrawala, Wilmot Li, and Floraine Berthouzoz. Design principles for visual communication. *Commun. ACM*, 54(4):60–69, April 2011.

[8] Maneesh Agrawala, Doantam Phan, Julie Heiser, John Haymaker, Jeff Klingner, Pat Hanrahan, and Barbara Tversky. Designing effective step-by-step assembly instructions. In *ACM Transactions on Graphics (TOG)*, volume 22, pages 828–837. ACM, 2003.

[9] Dror Aiger, Niloy J Mitra, and Daniel Cohen-Or. 4-points congruent sets for robust pairwise surface registration. *ACM Transactions on Graphics (TOG)*, 27(3):85, 2008.

[10] E. Altantsetseg, Y. Muraki, F. Chiba, and K. Konno. 3d surface reconstruction of stone tools by using four-directional measurement machine. *International Journal of Virtual Reality*, 10(1):37–43, 2011.

[11] Enkhbayar Altantsetseg, Katsutsugu Matsuyama, and Kouichi Konno. Pairwise matching of 3d fragments using fast fourier transform. *The Visual Computer*, 30(6-8):929–938, 2014.

[12] Enkhbayar Altantsetseg, Yuta Muraki, Katsutsugu Matsuyama, and Kouichi Konno. Feature line extraction from unorganized noisy point clouds using truncated fourier series. *The Visual Computer*, 29(6-8):617–626, 2013.

[13] Lucia Arbace, Elisabetta Sonnino, Marco Callieri, Matteo Dellepiane, Matteo Fabbri, Antonio Iaccarino Idelson, and Roberto Scopigno. Innovative uses of 3d digital technologies to assist the restoration of a fragmented terracotta statue. *Journal of Cultural Heritage*, 14(4):332–345, 2013.

[14] Jean-Paul Balabanian, Ivan Viola, and Eduard Gröller. Interactive illustrative visualization of hierarchical volume data. In *Proceedings of Graphics Interface 2010*, pages 137–144. Canadian Information Processing Society, 2010.

[15] Carlos Sánchez Belenguer and Eduardo Vendrell Vidal. Archaeological fragment characterization and 3d reconstruction based on projective gpu depth maps. In *Virtual Systems and Multimedia (VSMM), 2012 18th International Conference on*, pages 275–282. IEEE, 2012.

[16] Paul J Besl and Neil D McKay. Method for registration of 3-d shapes. In *Robotics-DL tentative*, pages 586–606. International Society for Optics and Photonics, 1992.

[17] Sofien Bouaziz, Andrea Tagliasacchi, and Mark Pauly. Sparse iterative closest point. In *Computer graphics forum*, volume 32, pages 113–123. Wiley Online Library, 2013.

[18] Stephen Boyd and Lieven Vandenberghe. *Convex optimization*. Cambridge university press, 2004.

[19] Knut Bretzke and Nicholas J Conard. Evaluating morphological variability in lithic assemblages using 3d models of stone artifacts. *Journal of Archaeological Science*, 39(12):3741–3749, 2012.

[20] Benedict J Brown, Corey Toler-Franklin, Diego Nehab, Michael Burns, David Dobkin, Andreas Vlachopoulos, Christos Doumas, Szymon Rusinkiewicz, and Tim Weyrich. A system for high-volume acquisition and matching of fresco fragments: Reassembling theran wall paintings. In *ACM Transactions on Graphics (TOG)*, volume 27, page 84. ACM, 2008.

[21] Stefan Bruckner and M Eduard Groller. Exploded views for volume data. *IEEE Transactions on Visualization and Computer Graphics*, 12(5), 2006.

[22] Chu-Song Chen, Yi-Ping Hung, and Jen-Bo Cheng. Ransac-based darces: A new approach to fast automatic registration of partially overlapping range images. *IEEE Transactions on Pattern Analysis and Machine Intelligence*, 21(11):1229–1234, 1999.

[23] Elvis C. S. Chen, A. Jonathan McLeod, John S. H. Baxter, and Terry M. Peters. Registration of 3d shapes under anisotropic scaling. *International Journal of Computer Assisted Radiology and Surgery*, 10(6):867–878, 2015.

[24] F Chiba, S Yokokoyama, A Kaneda, and K Konno. Development of network-type archaeological investigation system. *The International Archives of Photogrammetry, Remote Sensing and Spatial Information Sciences*, 40(5):99, 2015.

[25] Fumito Chiba and R Yokoyama. New method to generate excavation charts by openness operators. In *Proceedings of the 22nd CIPA Symposium, Kyoto, Japan*, volume 1115, page 15, 2009.

[26] A. Chida, K. Matsuyama, F. Chiba, and K. Konno. A rapid searching method of adjacent flake surfaces in stone implements by using sets of measured points for generating a joining material. *The Journal of the Society for Art and Science*, 13(2):107–115, 2014.

[27] Chris Clarkson, Lucio Vinicius, and Marta Mirazon Lahr. Quantifying flake scar patterning on cores using 3d recording techniques. *Journal of Archaeological Science*, 33(1):132–142, 2006.

[28] Andrea Frome, Daniel Huber, Ravi Kolluri, Thomas Bülow, and Jitendra Malik. Recognizing objects in range data using regional point descriptors. In *European conference on computer vision*, pages 224–237. Springer, 2004.

[29] Chi-Wing Fu, Peng Song, Xiaoqi Yan, Lee Wei Yang, Pradeep Kumar Jayaraman, and Daniel Cohen-Or. Computational interlocking furniture assembly. *ACM Transactions on Graphics (TOG)*, 34(4):91, 2015.

[30] Thomas Funkhouser, Hijung Shin, Corey Toler-Franklin, Antonio García Castañeda, Benedict Brown, David Dobkin, Szymon Rusinkiewicz, and Tim Weyrich. Learning how to match fresco fragments. *Journal on Computing and Cultural Heritage (JOCCH)*, 4(2):7, 2011.

[31] Leonardo Gomes, Olga Regina Pereira Bellon, and Luciano Silva. 3d reconstruction methods for digital preservation of cultural heritage: A survey. *Pattern Recognition Letters*, 50:3–14, 2014.

[32] Leore Grosman, Oded Smikt, and Uzy Smilansky. On the application of 3-d scanning technology for the documentation and typology of lithic artifacts. *Journal of Archaeological Science*, 35(12):3101–3110, 2008.

[33] Yulan Guo, Mohammed Bennamoun, Ferdous Sohel, Min Lu, Jianwei Wan, and Ngai Ming Kwok. A comprehensive performance evaluation of 3d local feature descriptors. *International Journal of Computer Vision*, 116(1):66–89, 2016.

[34] Yulan Guo, Ferdous Sohel, Mohammed Bennamoun, Min Lu, and Jianwei Wan. Rotational projection statistics for 3d local surface description and object recognition. *International journal of computer vision*, 105(1):63–86, 2013.

[35] Yulan Guo, Ferdous Ahmed Sohel, Mohammed Bennamoun, Min Lu, and Jianwei Wan. Trisi: A distinctive local surface descriptor for 3d

modeling and object recognition. In *GRAPP/IVAPP*, pages 86–93, 2013.

[36] James N Hill and Robert K Evans. A model for classification and typology. *Models in archaeology*, 351:73, 1972.

[37] Hugues Hoppe, Tony DeRose, Tom Duchamp, John McDonald, and Werner Stuetzle. *Surface reconstruction from unorganized points*, volume 26. ACM, 1992.

[38] Hui Huang, Minglun Gong, Daniel Cohen-Or, Yaobin Ouyang, Fuwen Tan, and Hao Zhang. Field-guided registration for feature-conforming shape composition. *ACM Transactions on Graphics (TOG)*, 31(6):179, 2012.

[39] Hui Huang, Shihao Wu, Minglun Gong, Daniel Cohen-Or, Uri Ascher, and Hao Richard Zhang. Edge-aware point set resampling. *ACM Transactions on Graphics (TOG)*, 32(1):9, 2013.

[40] Qi-Xing Huang, Simon Flöry, Natasha Gelfand, Michael Hofer, and Helmut Pottmann. Reassembling fractured objects by geometric matching. In *ACM Transactions on Graphics (TOG)*, volume 25, pages 569–578. ACM, 2006.

[41] A. Igarashi. Analytical reviews of conjoinable stone artefacts from palaeolithic sites in japan. *The historical science*, 67(3):465–488, 1998.

[42] Akira Igarashi. *Sekki zukuri no ziken koukogaku (Experimental archeology of the Stone tool Making)*, chapter Hakuhen hakuri genri: Seisei no zengo kankei (Flakes peeling principle: The context of generation), pages 22–35. Gakuseisha, Tokyo, JP, 2004.

[43] Yuki Igarashi, Takeo Igarashi, and Jun Mitani. Beady: interactive beadwork design and construction. *ACM Transactions on Graphics (TOG)*, 31(4):49, 2012.

[44] Marie-Louise Inizan, Mich 竪 le Reduron-Ballinger, H 辿 l 竪 ne Roche, and Jacques Tixier. *Technology and terminology of knapped stone*. Cercle de Recherches et d'Etudes Prehist, 1999.

[45] Olga Karpenko, Wilmot Li, Niloy Mitra, and Maneesh Agrawala. Exploded view diagrams of mathematical surfaces. *IEEE Transactions on Visualization and Computer Graphics*, 16(6):1311–1318, 2010.

[46] Florian Kleber, Markus Diem, Robert Sablatnig, and Martin Kampel. Proposing features for the reconstruction of marble plates of ephesos. In *Virtual Systems and Multimedia (VSMM), 2010 16th International Conference on*, pages 328–331. IEEE, 2010.

[47] Manfred Lau, Akira Ohgawara, Jun Mitani, and Takeo Igarashi. Converting 3d furniture models to fabricatable parts and connectors. *ACM Transactions on Graphics (TOG)*, 30(4):85, 2011.

[48] KH Lee, H Woo, and T Suk. Data reduction methods for reverse engineering. *The International Journal of Advanced Manufacturing Technology*, 17(10):735–743, 2001.

[49] Marc Levoy, Kari Pulli, Brian Curless, Szymon Rusinkiewicz, David Koller, Lucas Pereira, Matt Ginzton, Sean Anderson, James Davis, Jeremy Ginsberg, et al. The digital michelangelo project: 3d scanning of large statues. In *Proceedings of the 27th annual conference on Computer graphics and interactive techniques*, pages 131–144. ACM Press/Addison-Wesley Publishing Co., 2000.

[50] Wilmot Li, Maneesh Agrawala, Brian Curless, and David Salesin. Automated generation of interactive 3d exploded view diagrams. In *ACM Transactions on Graphics (TOG)*, volume 27, page 101. ACM, 2008.

[51] Sam CH Lin, Matthew J Douglass, Simon J Holdaway, and Bruce Floyd. The application of 3d laser scanning technology to the assessment of ordinal and mechanical cortex quantification in lithic analysis. *Journal of Archaeological Science*, 37(4):694–702, 2010.

[52] Zhen-Bao Liu, Shu-Hui Bu, Kun Zhou, Shu-Ming Gao, Jun-Wei Han, and Jun Wu. A survey on partial retrieval of 3d shapes. *Journal of Computer Science and Technology*, 28(5):836–851, 2013.

[53] Matthew Magnani. Three-dimensional alternatives to lithic illustration. *Advances in Archaeological Practice*, 2(4):285–297, 2014.

[54] Z. C. Marton, R. B. Rusu, and M. Beetz. On fast surface reconstruction methods for large and noisy point clouds. pages 3218–3223, 2009.

[55] K. Matsufuji and S. Monta. *Yoku wakaru koukogaku (Understand archeology)*, pages 18–18. Minerva Shobo, Kyoto, JP, 2010.

[56] Pavlos Mavridis, Anthousis Andreadis, and Georgios Papaioannou. Efficient sparse icp. *Computer Aided Geometric Design*, 35:16–26, 2015.

[57] Pavlos Mavridis, Ivan Sipiran, Anthousis Andreadis, and Georgios Papaioannou. Object completion using k-sparse optimization. In *Computer Graphics Forum*, volume 34, pages 13–21. Wiley Online Library, 2015.

[58] Nicolas Mellado, Dror Aiger, and Niloy J Mitra. Super 4pcs fast global pointcloud registration via smart indexing. In *Computer Graphics Forum*, volume 33, pages 205–215. Wiley Online Library, 2014.

[59] Niloy J Mitra, An Nguyen, and Leonidas Guibas. Estimating surface normals in noisy point cloud data. *International Journal of Computational Geometry & Applications*, 14(04n05):261–276, 2004.

[60] Niloy J. Mitra, Yong-Liang Yang, Dong-Ming Yan, Wilmot Li, and Maneesh Agrawala. Illustrating how mechanical assemblies work. *ACM Transactions on Graphics*, 29(3):58:1–58:12, 2010.

[61] Paula Monteiro. Computer graphics in archaeology.

[62] Michela Mortara, Chiara Eva Catalano, Francesco Bellotti, Giusy Fiucci, Minica Houry-Panchetti, and Panagiotis Petridis. Learning cultural heritage by serious games. *Journal of Cultural Heritage*, 15(3):318–325, 2014.

[63] Ed. Muraki. Excavation investigation report of OROSE. Technical report, Iwate Cultural Promotion Agency, Iwate, JP, 2013.

[64] Zdeňka Nerudová and Petr Neruda. Technology of moravian early szeletian leaf point shaping: A case study of refittings from moravskỳ krumlov iv open-air site (czech republic). *Quaternary International*, 2015.

[65] Zdeňka Nerudová and Petr Neruda. Technology of moravian early szeletian leaf point shaping: A case study of refittings from moravskỳ krumlov iv open-air site (czech republic). *Quaternary International*, 428:91–108, 2017.

[66] Anh Nguyen and Bac Le. 3d point cloud segmentation: A survey. In *Robotics, Automation and Mechatronics (RAM), 2013 6th IEEE Conference on*, pages 225–230. IEEE, 2013.

[67] R. Osada, T. Funkhouser, B. Chazelle, and D. Dobkin. Matching 3d models with shape distributions. pages 154–166, 2001.

[68] Gregorio Palmas, Nico Pietroni, Paolo Cignoni, and Roberto Scopigno. A computer-assisted constraint-based system for assembling fragmented objects. In *Digital Heritage International Congress (DigitalHeritage), 2013*, volume 1, pages 529–536. IEEE, 2013.

[69] Georgios Papaioannou, Evaggelia-Aggeliki Karabassi, and Theoharis Theoharis. Reconstruction of three-dimensional objects through matching of their parts. *IEEE TRANS. PAMI*, 24:2002, 2002.

[70] Kyoungju Park, April Nowell, and Dimitris Metaxas. Deformable model based shape analysis stone tool application. In *Computer Vision and Pattern Recognition Workshop, 2003. CVPRW'03. Conference on*, volume 1, pages 6–6. IEEE, 2003.

[71] Hanspeter Pfister, Matthias Zwicker, Jeroen Van Baar, and Markus Gross. Surfels: Surface elements as rendering primitives. In *Proceedings of the 27th annual conference on Computer graphics and interactive techniques*, pages 335–342. ACM Press/Addison-Wesley Publishing Co., 2000.

[72] Ruggero Pintus, Kazim Pal, Ying Yang, Tim Weyrich, Enrico Gobbetti, and Holly Rushmeier. A survey of geometric analysis in cultural heritage. In *Computer Graphics Forum*, volume 35, pages 4–31. Wiley Online Library, 2016.

[73] Samantha Thi Porter, Morgan Roussel, and Marie Soressi. A simple photogrammetry rig for the reliable creation of 3d artifact models in

the field: lithic examples from the early upper paleolithic sequence of les cottés (france). *Advances in Archaeological Practice*, 4(1):71–86, 2016.

[74] Eitan Richardson, Leore Grosman, Uzy Smilansky, and Michael Werman. Extracting scar and ridge features from 3d-scanned lithic artifacts. *Archaeology in the Digital Era*, page 83, 2014.

[75] Andrew T. R. Riddle and Michael Chazan. Stone tools from the inside out: radial point distribution. *World Archaeology*, 46(1):123–136, 2014.

[76] Ferran Roure, Xavier Lladó, Josep Forest, Tomislav Pribanic, and Joaquim Salvi. An experimental benchmark for point set coarse matching.

[77] Szymon Rusinkiewicz and Marc Levoy. Efficient variants of the icp algorithm. In *3-D Digital Imaging and Modeling, 2001. Proceedings. Third International Conference on*, pages 145–152. IEEE, 2001.

[78] Radu Bogdan Rusu, Nico Blodow, and Michael Beetz. Fast point feature histograms (fpfh) for 3d registration. In *Robotics and Automation, 2009. ICRA '09. IEEE International Conference on*, pages 3212–3217. IEEE, 2009.

[79] Samuele Salti, Federico Tombari, and Luigi Di Stefano. Shot: Unique signatures of histograms for surface and texture description. *Computer Vision and Image Understanding*, 125:251–264, 2014.

[80] M. Sato, K. Matsuyama, F. Chiba, and K. Konno. A method of restructuring a peel surface from unifying adjacent flakes to restore refitted flakes. In *NICOGRAPH 2012*, pages 70–73, 2012.

[81] Roberto Scopigno. Sampled 3d models for cultural heritage: which uses beyond visualization? *Virtual Archaeology Review*, 3(5):109–115, 2012.

[82] Roberto Scopigno, Marco Callieri, Paolo Cignoni, Massimiliano Corsini, Matteo Dellepiane, Federico Ponchio, and Guido Ranzuglia. 3d models for cultural heritage: Beyond plain visualization. *Computer*, 44(7):48–55, 2011.

[83] Roberto Scopigno, Marco Callieri, Paolo Cignoni, Massimiliano Corsini, Matteo Dellepiane, Federico Ponchio, and Guido Ranzuglia. 3d models for cultural heritage: Beyond plain visualization. *Computer*, 44(7):48–55, 2011.

[84] U. Sergey. Region growing segmentation. `http://www.pointclouds.org/documentation/tutorials/region_growing_segmentation.php`, 2015.

[85] Michael Shott. Digitizing archaeology: a subtle revolution in analysis. *World Archaeology*, 46(1):1–9, 2014.

[86] Michael J Shott and Kathryn J Weedman. Measuring reduction in stone tools: an ethnoarchaeological study of gamo hidescrapers from ethiopia. *Journal of Archaeological Science*, 34(7):1016–1035, 2007.

[87] Mofei Song, Zhengxing Sun, Kai Liu, and Xufeng Lang. Iterative 3d shape classification by online metric learning. *Computer Aided Geometric Design*, 35:192–205, 2015.

[88] Peng Song and Xiaoping Chen. Pairwise surface registration using local voxelizer. 2015.

[89] T AlExAndrA SuMnEr and Andrew TR Riddle. A virtual paleolithic: assays in photogrammetric three-dimensional artifact modelling. *PaleoAnthropology*, 2008:158–169, 2008.

[90] K. Suzuki. *Koukogaku nyuumon (Archaeology Introduction)*. University of Tokyo Press, Kyoto, JP, 1988.

[91] Yamamoto T. *Dictionary of Japanese Archaeological Terms*. Tokyo Bijutsu, Kyoto, JP, 2001.

[92] Markus Tatzgern, Denis Kalkofen, and Dieter Schmalstieg. Compact explosion diagrams. In *Proceedings of the 8th International Symposium on Non-Photorealistic Animation and Rendering*, pages 17–26. ACM, 2010.

[93] Corey Toler-Franklin, Benedict Brown, Tim Weyrich, Thomas Funkhouser, and Szymon Rusinkiewicz. Multi-feature matching of fresco fragments. In *ACM Transactions on Graphics (TOG)*, volume 29, page 185. ACM, 2010.

[94] Federico Tombari, Samuele Salti, and Di Luigi Stefano. Unique shape context for 3d data description. In *3DOR '10 Proceedings of the ACM workshop on 3D object retrieval*, pages 57–62. ACM, 2010.

[95] Daniel Wickeroth, Andreas Pastoors, Dominik Laurentius, and Ulrich Lang. Artefactviewer-a 3d tool for archeologists. In *Digital Heritage, 2015*, volume 2, pages 435–438. IEEE, 2015.

[96] Andrew R Willis. Computational analysis of archaeological ceramic vessels and their fragments. *Digital Imaging for Cultural Heritage Preservation: Analysis, Restoration, and Reconstruction of Ancient Artworks*, page 323, 2011.

[97] S. Winkelbach and F. M Wahl. Pairwise matching of 3d fragments using cluster trees. *International Journal of Computer Vision*, 78(1):1–13, 2008.

[98] Shiqing Xin, Chi-Fu Lai, Chi-Wing Fu, Tien-Tsin Wong, Ying He, and Daniel Cohen-Or. Making burr puzzles from 3d models. In *ACM Transactions on Graphics (TOG)*, volume 30, page 97. ACM, 2011.

[99] K. Yamahara, K. Konno, F. Chiba, and M. Satoh. A method of detecting adjacent flakes in stone tool restoration by extracting peeling surfaces. *The information archaeology*, 17(1-2):23–31, 2011.

[100] Jiaolong Yang, Hongdong Li, Dylan Campbell, and Yunde Jia. Go-icp: a globally optimal solution to 3d icp point-set registration. *IEEE transactions on pattern analysis and machine intelligence*, 38(11):2241–2254, 2016.

[101] Jiaqi Yang, Zhiguo Cao, and Qian Zhang. A fast and robust local descriptor for 3d point cloud registration. *Information Sciences*, 346:163–179, 2016.

[102] X. Yang, K. Matsuyama, K. Konno, and Tokuyama Y. Feature-preserving simplification of point cloud by using clustering approach based on mean curvature. *The Journal of the Society for Art and Science*, 14(4):117–128, 2015.

[103] Xi Yang, Katsutsugu Matsuyama, and Kouichi Konno. A new method of refitting mixture lithic materials by geometric matching of flake surfaces. *The Journal of Art and Science*, 15(4):167–176, 2016.

[104] Xi Yang, Katsutsugu Matsuyama, and Kouichi Konno. Interactive visualization of assembly instruction for stone tools restoration. In *Pacific Visualization Symposium (PacificVis), 2017 IEEE*, pages 270–274. IEEE, 2017.

[105] Chunjia Zhang, Shaoyi Du, Juan Liu, Yongxin Li, Jianru Xue, and Yuehu Liu. Robust iterative closest point algorithm with bounded rotation angle for 2d registration. *Neurocomputing*, 195:172–180, 2016.

[106] Yu Zhong. Intrinsic shape signatures: A shape descriptor for 3d object recognition. In *Computer Vision Workshops (ICCV Workshops), 2009 IEEE 12th International Conference on*, pages 689–696. IEEE, 2009.

# List of Publications

- X.Yang, K. Matsuyama, K. Konno: "A New Method of Refitting Mixture Lithic Materials by Geometric Matching of Flake Surfaces ", *The Journal of Art and Science*, Vol.15, No. 4, pp.167-176, 2016.
- X. Yang, K. Matsuyama, K. Konno, F. Chiba, S. Yokoyama: "Analysis and Visualization Instruction by Flake Knapping Sequence for Chipped Stone Tools", *NICOGRAPH 2017*, 2017.
- X. Yang, K. Matsuyama, K. Konno: "Pairwise Matching of Stone Tools Based on Flake-Surface Contour Points and Normals", *Eurographics Workshop on Graphics and cultural Heritage*, The Eurographics Association, 2017.
- X. Yang, K. Matsuyama, K. Konno: "Interactive Visualization of Assembly Instruction for Stone Tools Restoration", *The 10th IEEE Pacific Visualization Symposium (PacificVis 2017)*, pp.270-274, 2017.